Nuclear AGO1 Regulates Gene Expression by Affecting Chromatin Architecture in Human Cells

Article

Cell Systems

Nuclear AGO1 Regulates Gene Expression by Affecting Chromatin Architecture in Human Cells

Graphical Abstract

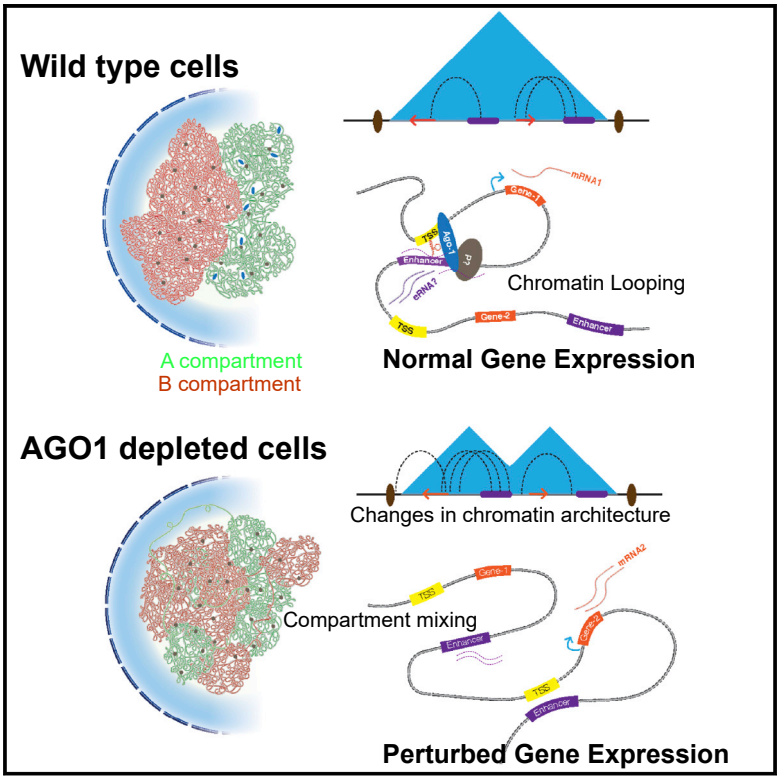

Authors

Muhammad Shuaib,
Krishna Mohan Parsi,
Manjula Thimma, ..., Timothy Ravasi,
Piero Carninci, Valerio Orlando

Correspondence

valerio.orlando@kaust.edu.sa

In Brief

Shuaib et al. used genome-wide approaches to investigate the role of nuclear AGO1 in chromatin organization and gene expression regulation in human cells. Depletion of AGO1 causes differential gene expression and disorganization of 3D chromatin structure such as loss and gain of chromosomal interactions, changes in the compartment, and eRNA, primarily in the AGO1 binding regions.

Highlights

- AGO1 enrichment on chromatin and transcriptional enhancers is mediated by eRNAs
- AGO1 depletion alters global transcriptional output including eRNA transcripts
- Enhancer-associated AGO1 contributes to the maintenance of 3D chromatin organization

Shuaib et al., 2019, Cell Systems 9, 446–458
November 27, 2019
https://doi.org/10.1016/j.cels.2019.09.005

CellPress

OPEN ACCESS
CellPress

Cell Systems
Article

Nuclear AGO1 Regulates Gene Expression by Affecting Chromatin Architecture in Human Cells

Muhammad Shuaib,[1,8] Krishna Mohan Parsi,[2,8] Manjula Thimma,[1] Sabir Abdu Adroub,[1] Hideya Kawaji,[3,5,6,7] Loqmane Seridi,[1] Yanal Ghosheh,[1] Alexandre Fort,[3] Bodor Fallatah,[1] Timothy Ravasi,[4] Piero Carninci,[3,5] and Valerio Orlando[1,2,9,*]

[1]King Abdullah University Science and Technology (KAUST), BESE Division, KAUST Environmental Epigenetics Program, Thuwal 23955-6900, Saudi Arabia
[2]IRCSS Fondazione, Santa Lucia, Epigenetics and Genome Reprogramming, Rome, Italy
[3]RIKEN Center for Life Science Technologies, Division of Genomic Technologies, 1-7-22 Suehiro-cho, Tsurumi-ku, Yokohama, Kanagawa 230-0045, Japan
[4]Marine Climate Change Unit, Okinawa Institute of Science and Technology Graduate University (OIST), 1919-1 Tancha, Onna-son, Okinawa 904-0495, Japan
[5]RIKEN Center for Integrative Medical Sciences, 1-7-22 Suehiro-cho, Tsurumi-ku, Yokohama, Kanagawa 230-0045, Japan
[6]RIKEN Preventive Medicine and Diagnosis Innovation Program, 2–1 Hirosawa, Wako, Saitama 351-0198, Japan
[7]Tokyo Metropolitan Institute of Medical Science, 2-1-6 Kamikitazawa, Setagaya-ku, Tokyo 156-8506, Japan
[8]These authors contributed equally
[9]Lead Contact
*Correspondence: valerio.orlando@kaust.edu.sa
https://doi.org/10.1016/j.cels.2019.09.005

SUMMARY

The impact of mammalian RNA interference components, particularly, Argonaute proteins, on chromatin organization is unexplored. Recent reports indicate that AGO1 association with chromatin appears to influence gene expression. To uncover the role of AGO1 in the nucleus, we used a combination of genome-wide approaches in control and AGO1-depleted HepG2 cells. We found that AGO1 strongly associates with active enhancers and RNA being produced at those sites. Hi-C analysis revealed AGO1 enrichment at the boundaries of topologically associated domains (TADs). By Hi-C in AGO1 knockdown cells, we observed changes in chromatin organization, including TADs and A/B compartment mixing, specifically in AGO1-bound regions. Distinct groups of genes and especially eRNA transcripts located within differentially interacting loci showed altered expression upon AGO1 depletion. Moreover, AGO1 association with enhancers is dependent on eRNA transcription. Collectively, our data suggest that enhancer-associated AGO1 contributes to the fine-tuning of chromatin architecture and gene expression in human cells.

INTRODUCTION

Argonaute (AGO) proteins are key members of the RNA interference (RNAi) pathway and are well documented for their role in small RNA-mediated post-transcriptional gene silencing in the cytoplasm (Meister, 2013; Joshua-Tor and Hannon, 2011). In fission yeast, AGO proteins and small RNAs are essential for heterochromatin formation (Volpe et al., 2002) and, similarly, in plants, for RNA-dependent DNA methylation (Zilberman et al., 2003). However, the function of RNAi components in animal cell chromatin organization-mediated transcriptional regulation remains unclear. We previously reported that in *Drosophila*, RNAi components (dAgo2 and Dicer) are preferentially associated with active chromatin and affect transcription by regulating RNA pol II pausing and stress response (Cernilogar et al., 2011). Another report indicated that in *Drosophila,* dAgo2 associates with insulator proteins CTCF and CP190 at active promoters and controls looping interactions between insulators, promoters, and enhancers (Moshkovich et al., 2011). In human cells, AGO1 binds to RNA pol II (Huang et al., 2013) to associate with active promoters, enhancers (Alló et al., 2014), HP1α, and CTCF (Agirre et al., 2015) and affects splicing (Alló et al., 2014; Ameyar-Zazoua et al., 2012; Agirre et al., 2015). However, the role of chromatin-associated AGO1 in regulating gene expression remains to be elucidated. A study showed AGO1 binding with RNA polymerase II and active promoters (Huang et al., 2013), while another report indicated that AGO1 association with active enhancers did not explain the observed widespread changes in gene expression in AGO1 depleted cells (Alló et al., 2014). In particular, it seemed important to understand whether enhancer-associated AGO1 can directly or indirectly impact transcription.

Enhancers are cis-regulatory elements in the mammalian genome that orchestrate gene expression programs by direct looping or indirect contacts with target gene promoters (Bulger and Groudine, 2011; Ong and Corces, 2011). Enhancer loci generally undergo bidirectional transcription by RNA pol II to produce enhancer RNAs (eRNAs) (Natoli and Andrau, 2012). The association of AGO1 with active enhancers was postulated

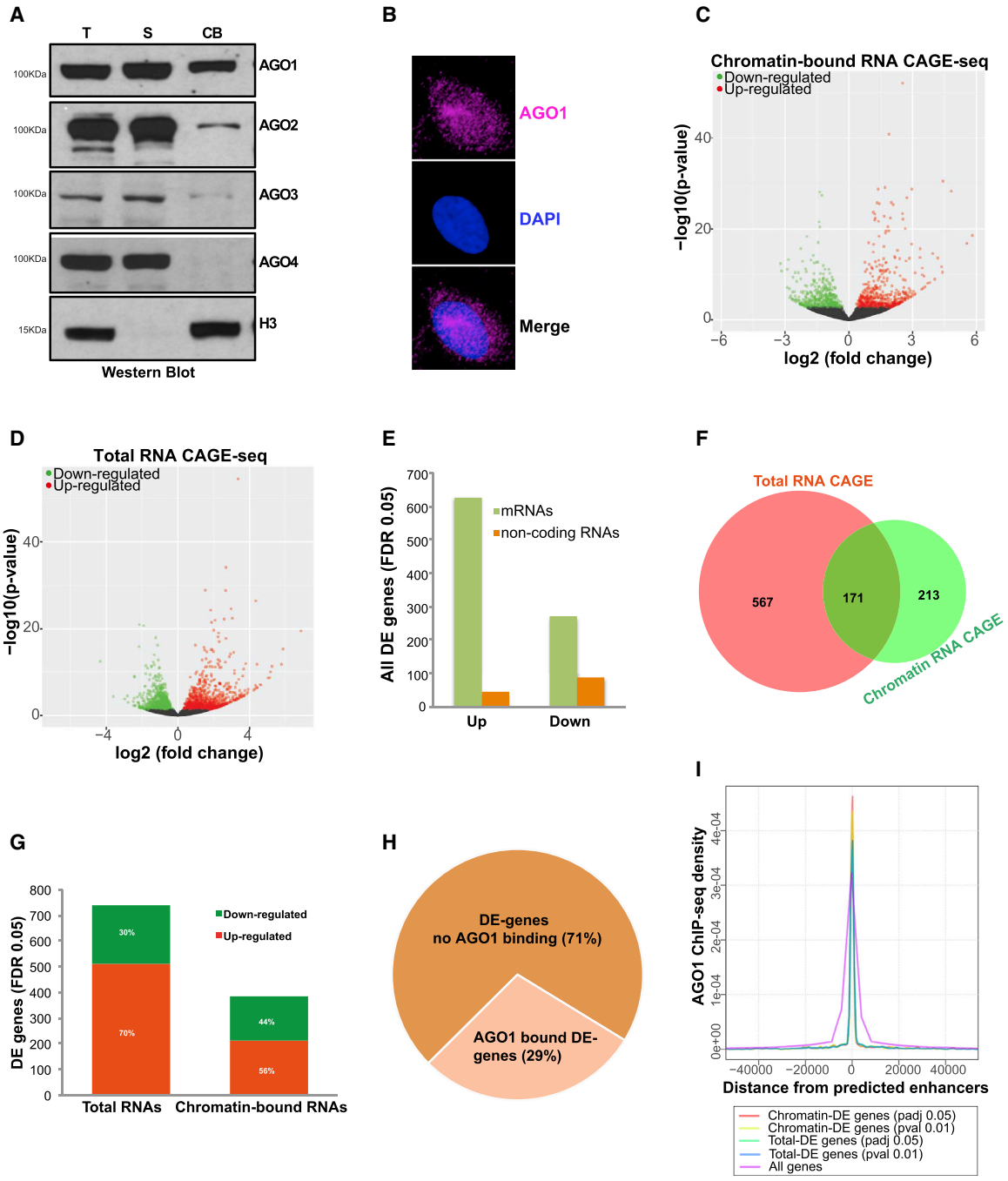

Figure 1. AGO1 Associates with Chromatin and Its Depletion Results in Deregulation of Coding and Non-coding Transcripts

(A) HepG2 cellular fractionation and western blotting using specific antibodies to detect AGO1, AGO2, AGO3, and AGO4 in different subcellular fractions (T = total, S = soluble, and CB = chromatin bound). H3 was used as a chromatin marker.

(B) Detection of AGO1 nuclear localization in HepG2 cells, by immunofluorescence analysis. AGO1 specific antibody detects both chromatin-associated and cytoplasmic endogenous AGO1. DAPI was used to stained nuclei (blue).(C and D) Volcano plots showing differentially expressed genes in AGO1 depleted cells, identified by CAGE-seq analysis from chromatin associated RNAs (C) and total RNAs (D). Downregulated genes (green) and upregulated genes are shown in (red).

(E) Bar plot illustrating number of all (total and chromatin associated combined together) significant (FDR 0.05) differentially expressed coding (mRNA) and non-coding genes.

(F) Venn diagram showing overlap of differentially expressed genes identified in total RNAs and chromatin associated RNAs by CAGE-seq analysis.

(G) Bar plot showing number significant (FDR 0.05) differentially expressed genes in each condition (total RNAs and chromatin-bound RNAs).

(legend continued on next page)

to be mediated by enhancer RNAs (Alló et al., 2014). Both enhancer elements and eRNAs are implicated in higher-order chromatin interactions that play an essential role in gene regulation (Hah et al., 2013). Recently, genome-wide chromosome conformation capture analysis (Hi-C) has revealed that chromosomes are organized into active (open, A-type) and inactive (closed, B-type) compartments (Lieberman-Aiden et al., 2009), which are further composed of clusters of interactions called topologically associated domains (TADs), separated by boundary regions (Dixon et al., 2012; Nora et al., 2012). The 3D chromatin structure is believed to regulate gene expression by establishing loops between enhancers and promoters and/or by bridging regulatory elements and genes into spatial chromatin hubs, compartments, and domains (Bouwman and de Laat, 2015). Several chromatin regulators, including polycomb proteins, cohesin, CTCF, and mediator complex have been reported to influence 3D genome organization (Sofueva et al., 2013; Zuin et al., 2014; Kagey et al., 2010; Seitan et al., 2013; Delest et al., 2012). However, a potential contribution of enhancer-associated AGO1 in three-dimensional chromatin (3D) organization has not yet been tested.

Here, by using a combination of genome-wide approaches, we provide evidence for an unexpected role of AGO1 in chromatin topological organization. We demonstrate that AGO1 binds at active chromatin regions mainly on proximal and distal enhancers. AGO1 depletion changes the 3D genome architecture leading to differential interactions, derangement of TADs configuration, and chromatin compartments that correlate with changes in gene expression. Collectively, these findings unveil an unprecedented link between enhancer-associated AGO1, the stability of higher-order chromatin architecture, and maintenance of proper gene expression program in human cells.

RESULTS

AGO1 Associates with Chromatin and Its Depletion Results in Deregulation of Coding and Non-coding Transcripts at Genome-wide Level

To understand the function of endogenous AGO proteins inside the nucleus, we first examined their nuclear and chromatin association. After cellular fractionation of HepG2 cells, the western blot analysis revealed that AGO1 was more enriched compared to AGO2-4 in the chromatin-bound fraction (Figure 1A). AGO1 nuclear distribution was further confirmed by immunofluorescence using AGO1-specific antibody (Figure 1B). Therefore, we focused our subsequent analysis only on AGO1 and its potential nuclear function. To evaluate the impact of AGO1 depletion on global transcriptional changes of all expressed TSS, we decided to use CAGE-seq analysis (Takahashi et al., 2012). We knocked down AGO1 with a pool of four siRNAs (siAGO1) and performed a control knockdown (KD) using a non-specific scrambled siRNA (siCtrl) in HepG2 cells. The efficiency of knockdown for each individual single siRNA was also tested. We confirmed the downregulation of AGO1 by western blot and immunofluorescence analysis (Figures S1A–S1C). AGO1-depleted cells showing a similar pattern of cell viability (Figure S1D) and cell-cycle profiles compared to control KD cells (Figure S1E) were processed for further analysis. We then applied CAGE-seq on total and chromatin extracted RNA from control (siCtrl) and AGO1 depleted (siAGO1) cells. All three replicates in each condition showed a similar clustering pattern between themselves as represented in PCA plot (Figure S1F). We identified more than 1,000 genes in both total and chromatin-bound RNA CAGE-seq data that were differentially expressed (DE) (Figures 1C–1E and for detail see Table S1). By comparing CAGE-seq data from total RNA and chromatin-bound RNA, we observed 171 common differentially expressed genes in the two fractions (Figure 1F). Considering only the highly perturbed genes (FDR $\leq$ 0.05), we found that 512 genes were upregulated, whereas 226 genes showed downregulation in total RNA-CAGE. Similarly, 213 upregulated genes and 170 downregulated genes were found in CAGE data from chromatin-bound RNAs (Figure 1G). These observations indicate that loss of AGO1 has both a positive and negative impact on gene expression (Figure 1G). We further extended our analysis to find a possible correlation between perturbed transcripts and deregulated miRNAs. To this, we compared small RNA-seq data with CAGE-seq in control and AGO1-depleted cells. The majority (95%) of perturbed mRNAs were not direct targets of differentially expressed miRNAs (Figures S2A–S2B). Moreover, we did not observe any good correlation between the effect of down and upregulated miRNAs and the expression of predicted targets (Figures S2C–S2E).

To discriminate between directly and indirectly regulated genes, we integrated CAGE-seq with AGO1 binding sites on chromatin (ChIP-seq). Among all the differentially expressed genes, we observed AGO1 binding at about 29% (274) genes, but only 16% (43) of these genes overlapped with AGO1 peaks at their promoters. In contrast, for the majority of perturbed genes (71%), we did not detect AGO1 at their promoters or within the coding region (Figure 1H). However, we observed a clear enrichment of AGO1 binding at the predicted enhancers located within <50 kb of all the differentially expressed genes (Figure 1I). These results suggest that AGO1 may alter predominant gene expression via binding at potential distal regulatory regions, though mechanistic aspects remained to be clarified.

The putative active enhancers are marked by bidirectional transcription of nuclear enhancer RNAs (eRNAs) that can be detected by CAGE (Andersson et al., 2014). By using chromatin CAGE-seq data, we identified 5,538 and 3,574 putative active eRNA loci in siCtrl and siAGO1 cells, respectively. Similarly, from total RNA CAGE, we identified 3,574 and 4,687 CAGE-predicted eRNAs in siCtrl and siAGO1 cells, respectively. To obtain information about eRNA dynamics upon AGO1 depletion, we focused on 573 (from chromatin) and 476 (from total) CAGE-identified eRNAs that were common between siCtrl and siAGO1

(H) Integration of ChIP-seq and AGO1-knockdown CAGE-seq data classify AGO1-responsive genes into direct and indirect targets. 29% of all differentially expressed (DE) genes (from total and chromatin CAGE-seq combined) contain AGO1 binding at their promoter or intragenically, represent direct targets. 71% do not overlap with AGO1 peaks (means indirect targets).

(I) Density plot of AGO1 ChIP-seq peaks closer than 50 kb to genes (either differentially expressed or considering all genes) centered at enhancer regions predicted by ChromHMM.

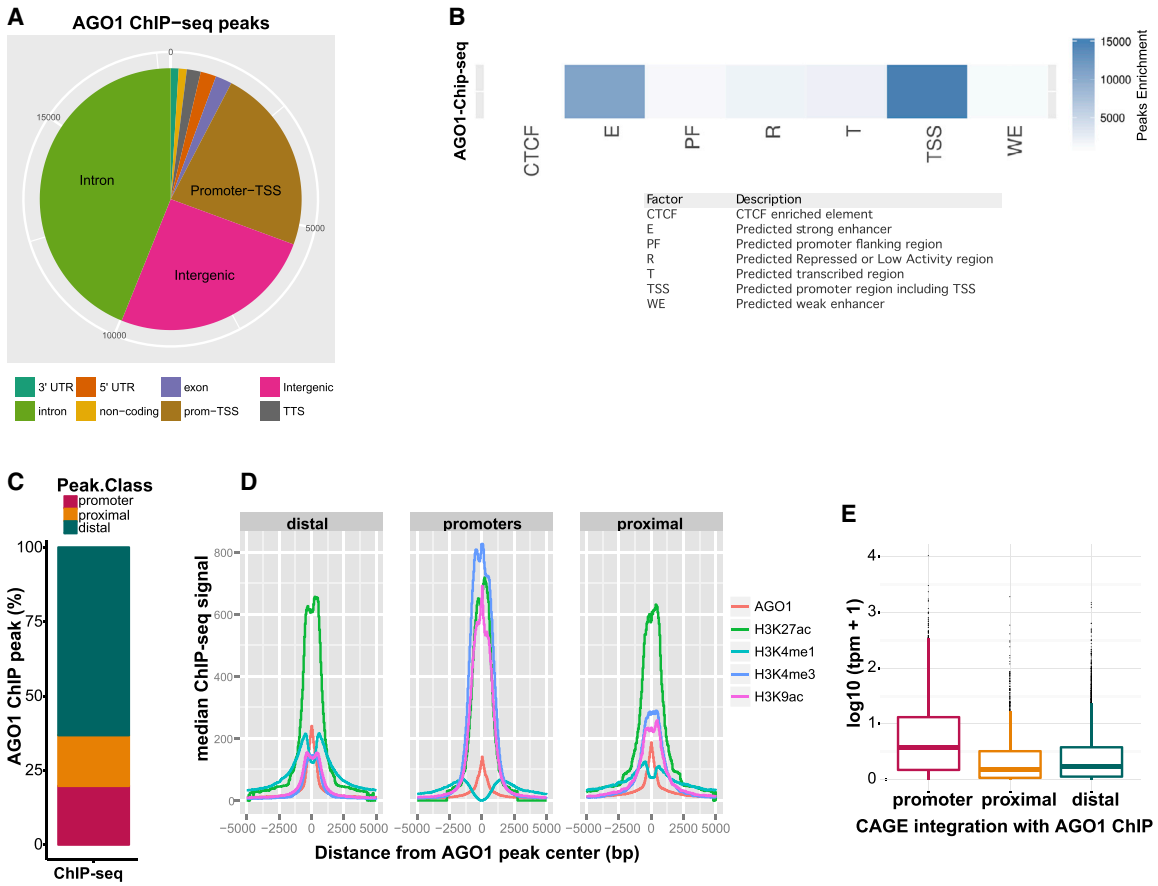

Figure 2. AGO1 Is Strongly Enriched at Transcriptionally Active Enhancers via RNA

(A) Pie chart representing the distribution of AGO1 ChIP-seq peaks relative to genes (located over UTRs, exons, introns, 2-kbp upstream regions [promoter-TSSs], 1-kbp downstream regions [TTSs]). The term "non-coding" refers to the exons of non-coding transcripts.

(B) Heatmap showing enrichment of AGO1 ChIP-seq peaks at active enhancers (E) and promoters (TSS) determined by overlapping ChIP-seq peaks with chromatin segmentation states (Hoffman et al., 2013) of HepG2 cells predicted by ChromHMM and Segway.

(C) Bar plot shows percent enrichment of AGO1 ChIP-seq peaks at distal, promoter, and proximal regions. AGO1 peaks are highly enriched in distal regions (i.e., >5 kb from nearest annotated TSS). AGO1 peaks also associate with promoter region (i.e., <1 kb from nearest annotated TSS).

(D) Density plot of ChIP-seq signals (median) of AGO1 and histone marks from ENCODE datasets including H3K4me1, H3K4me3, H3K9ac, and H3K27ac centered at AGO1 peak located in distal, proximal, and promoter regions. AGO1-bound distal regions are enriched with active enhancer marks such as H3K4me1, H3K27ac, and H3K4me3 representing transcriptionally active enhancers.

(E) Density of CAGE-seq signals represents transcriptional activity at AGO1-binding sites (promoter, proximal, and distal). The low level of transcriptional activity at AGO1-enriched distal regulatory elements indicates enhancer RNAs (eRNAs).

cells (for detail see Tables S2 and S3). We observed apparent differences in the expression level (TPM values, Tags Per Million) of eRNAs between siCtrl and siAGO1 cells (Figures S1G–S1H).

AGO1 Is Strongly Enriched at Transcriptionally Active Enhancers via RNA

To identify AGO1 genomic distribution in human HepG2 cells, we performed ChIP-seq (for antibody specificity, see Figures S1A–S1C). AGO1 ChIP-seq data analysis revealed approximately 80% mapping rate, and we identified 17,771 reproducible AGO1-specific peaks (for detailed AGO1 ChIP peak annotation, see Table S4). Examining the annotation of these peaks, we found AGO1 peak distribution in genic (introns and promoters) and inter-genic regions (Figure 2A; see Figure S3 for comparison of AGO1 and HA-AGO1 ChIP-seq). We validated the binding of AGO1 on selected target regions using ChIP-qPCR experiment in control and AGO1-depleted cells (Figures S4A and S4B and for detail of primer sequence used, see Table S5). The distribution of AGO1 peaks in intronic and intergenic regions (Figure 2A) may represent potential enhancers. Thus, we overlaid AGO1 ChIP-seq peaks with the chromatin states of HepG2 cells predicted by the combination of ChromHMM and Segway. Most represented classes were promoters and predicted strong enhancer regions (Figure 2B). We further categorized AGO1 peaks into three classes, i.e., promoter, proximal, and distal regions based on distance from TSS (promoter = 1kb up or downstream, proximal = within 5kb, and distal regions = 5kb up to 50kb). The majority of AGO1 peaks are associated with distal regions (Figure 2C). To check that these sites are indeed enhancers, we used publicly available ENCODE HepG2 histone ChIP-seq datasets associated with enhancer and promoter regions (H3K4me1, H3K4me3, H3K27ac, and H3K9ac).

AGO1-enriched promoter sites showed clear overlap with active TSS marks (H3K27ac, H3K9ac, and H3K4me3) but not with H3K4me1 (Figure 2D). The AGO1-bound distal regions overlapped active enhancer marks such as H3K4me1, H3K27ac, and H3K4me3 (Figure 2D). Next, by overlapping all expressed TSS tags from CAGE-seq with AGO1 peaks, we observed a clear correlation with RNAs produced at those sites (Figure 2E).

To clarify the involvement of RNAs in AGO1 chromatin association, we performed cross-linked AGO1 RIP-seq from chromatin-bound AGO1-associated RNAs in the nucleus. We then intersected all identified AGO1-associated RNA peaks (including coding, non-coding, and un-annotated peaks) with AGO1-bound (ChIP-seq) and -unbound chromosomal regions across the genome. We found enrichment of RNA peaks on AGO1-bound active sites when compared to AGO1-absent sites in the genome (Figure 3A). We next examined whether RNA binding of AGO1 contributes to its chromatin association. After chromatin fractionation in the presence and absence of RNase treatment, the level of AGO1 protein was detected by western blotting. We observed that RNase treatment highly reduced AGO1 protein level in the chromatin fraction (Figures 3B and 3C). Thus, RNA binding stabilizes AGO1 chromatin association.

The AGO1-enriched proximal and distal regions showed a low level of transcriptional activity that may represent putative enhancer RNAs (eRNAs) (Figure 2E). To investigate the association between chromatin-bound AGO1 and eRNAs, we first examined AGO1 binding at putative eRNAs loci identified by CAGE. We found a clear enrichment of AGO1 ChIP signals around chromatin CAGE-defined eRNAs midpoint (Figures 3D and 3E). We then intersected the chromatin CAGE-defined eRNA loci with our AGO1 binding sites (ChIP peaks). Of 5,538 CAGE-identified eRNA loci, 573 putative eRNAs exactly overlapped with AGO1-bound enhancer regions across the genome (Table S6). Next, we overlaid this list of 573 putative eRNAs with active enhancer marks H3K4me1 and H3K27ac (ENCODE HepG2 histone ChIP) and with GRO-seq data recently published in HepG2 cells (Bouvy-Liivrand et al., 2017). Among these, 94 CAGE-identified eRNAs overlapped with H3K4me1, H3K27ac, and GRO-seq peaks (Table S7). To validate the requirement of transcriptionally active eRNAs and enhancer-like long-non-coding RNAs (lncRNAs) for AGO1 enhancer association, we investigated AGO1 binding on some randomly selected enhancer loci (as defined by chromatin-CAGE, Table S7) upon inhibition of RNA polymerase II by actinomycin D treatment. Upon transcription inhibition, both eRNAs (sense and antisense) and AGO1 ChIP signals are significantly reduced in 9 selected CAGE-defined enhancer regions (Figures 3F and 3G), which certify AGO1 enrichment at transcriptionally active enhancers is mediated by eRNAs.

AGO1 Depletion Alters Chromatin Interactions Specifically in AGO1-Bound Regions

Since AGO1 binding at distal regulatory elements indirectly impacts global gene expression, we hypothesized a role of nuclear AGO1 in higher-order chromatin organization. To this scope, we performed an unbiased genome-wide chromatin conformation analysis using Hi-C in siCtrl and siAGO1 HepG2 cells (Figure S5). At the global level, the chromosomal interaction frequency heatmaps for each individual chromosome displayed similar patterns in both siAGO1 and siCtrl cells (Figures 4A and 4B). To gain deeper insight into differential interaction frequencies between siCtrl and siAGO1 cells, we compared normalized HiC data (siAGO1 versus siCtrl) with the R package diffHiC (Lun and Smyth, 2015). The diffHiC analysis revealed differences in genome-wide chromatin interactions between siAGO1 and siCtrl cells (Figures 4C and 4D). Upon AGO1 depletion, we observed extensive changes in both long-range and short-range interaction frequency across the genome (Figures 3C and 3D). Next, we asked whether changes in chromosomal interactions were correlated with AGO1 binding sites. We found that 93% of AGO1 binding sites (16,566 AGO1 peaks) overlapped with differential interacting regions at the genome-wide level (Figures 4E, S5F, and S5G). We then calculated the difference in the number of differential interactions between AGO1 enriched and without AGO1 binding 20-kb bins. We observed significantly (t test < 0.05) higher number of differential interactions between bin-pairs containing AGO1 binding sites than without AGO1 binding (Figure 4F). In particular, upon AGO1 depletion, we observed a decrease in chromosomal interaction frequency among AGO1 binding sites, with a simultaneous gain in chromatin interactions at other genomic loci (Figure 4G). Overall, these data suggest that AGO1 binding at genomic regulatory sites has influence on their higher-order chromatin interactions.

AGO1 Depletion Perturbs Compartments and TADs Organization at AGO1-Associated Genomic Regions

Models derived from omics data analysis (HiC) indicate that the genome is partitioned into active (open, A-type) and inactive (closed, B-type) compartments (Lieberman-Aiden et al., 2009; Rao et al., 2014). Thus, we first investigated the effects of AGO1 depletion on the A/B chromatin compartmentalization. We defined chromatin compartments (A and B) using the first principal component (PC1) by eigenvector analysis (Zhang et al., 2012). To further demarcate A/B chromatin compartments, we also intersected expressed genes (identified by CAGE-seq) with eigenvector values. We then compared the genome-wide compartments between siCtrl and siAGO1 cells at 100-kb resolution. The siAGO1 cells displayed a highly mixed A and B compartmentalization pattern (Figure 5A). We found that 14% of the siAGO1 genome showed compartments switching, which predominantly occurred in the AGO1-bound open A-type compartment (Figures 5B and 5C).

To examine the effect on TAD organization, we first identified 3,143 and 3,593 TADs in siCtrl and siAGO1 cells, respectively, using TADbit tool (Serra et al., 2016) (Figure 6A). Next, we assessed the distribution of TADs within A/B compartments. TADs were placed in either A or B compartment, then by comparing siAGO1 and siCtrl genome, we found that around 12% of TADs switched from A-type to B-type compartment at a genome-wide level (Figure 6B). We consistently found that in siAGO1 TADs size was smaller compared to siCtrl cells (t test, FDR < 0.05) (Figure 6C). Then, by visualizing the topological domains in AGO1-depleted cells, we frequently observed that larger domains found in siCtrl cells were divided into smaller sub-domains (Figure 6D). Additionally, we found that 25% of AGO1 binding sites (detected by ChIP-seq) overlapped with TAD boundaries identified at 100-kb resolution (Figure 6E).

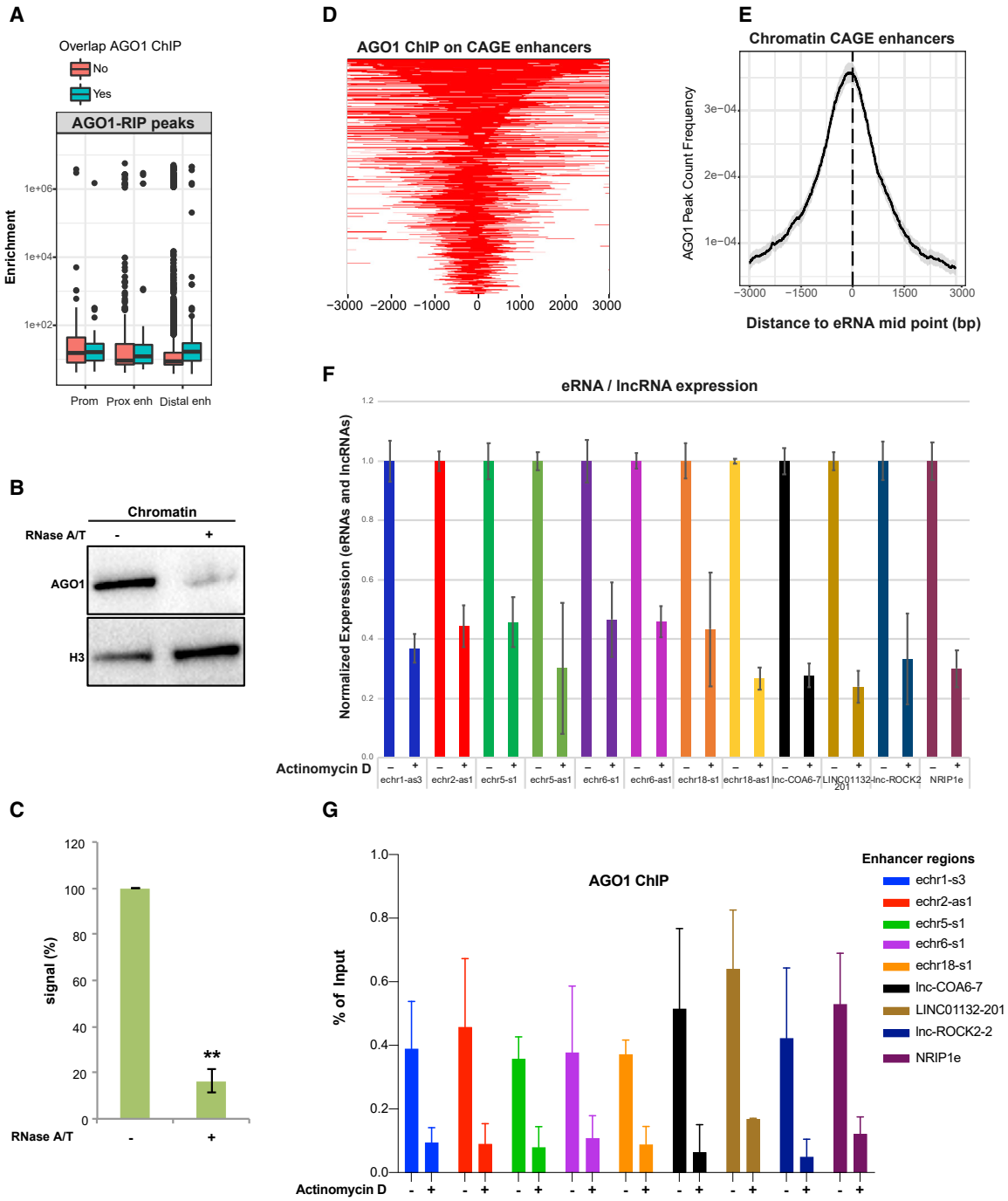

Figure 3. AGO1 Enrichment at Active Enhancers Is Dependent on eRNA

(A) The Box plot shows enrichment of RIP-seq peaks on AGO1 binding sites (promoter, proximal, and distal regions) (Mann-Whitney test, p value 4.4e-12).

(B and C) Western blot (B) and quantitative densitometry analysis (C) shows AGO1 association with chromatin in the presence and absence of RNase A/T1 treatment. H3 was used as loading marker. Densitometry analysis was performed from two independent experiments (as shown mean ± SD). (**$p < 0.01$, one-way ANOVA Dunnett post-hoc test).

(D and E) Heatmap (D) and metagene plot (E) showing AGO1 ChIP signal enrichment around chromatin-CAGE predicted eRNA-expressing enhancer regions (± 3kb).

(F and G) Effects of transcription inhibition in HepG2 cell by actinomycin D treatment (1.6 μM for 6 h) on the expression level (F) of CAGE-identified eRNAs or lncRNAs and (G) AGO1 occupancy (ChIP signal) within these enhancer regions. The RNA expression level and DNA from AGO1 ChIP were quantified by qPCR (± SD from 2 independent experiments). Primers used are listed in Table S5.

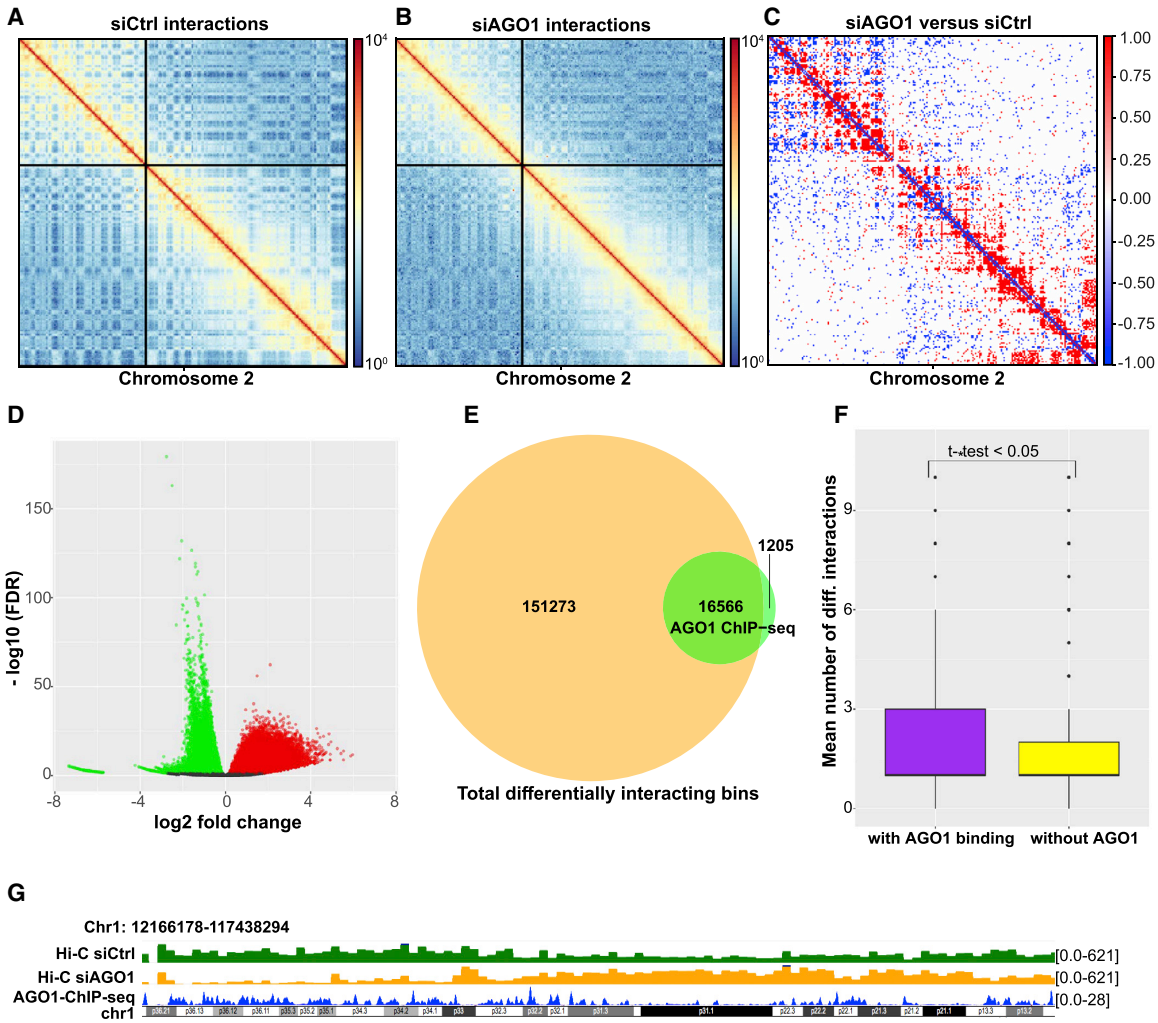

Figure 4. AGO1 Depletion Alters Chromatin Interactions Specifically in AGO1-bound Regions

(A and B) Genome-wide chromatin conformation Hi-C analysis was performed using two replicates of siCtrl and siAGO1 cells. Representative normalized Hi-C interaction heatmaps of chromosome 2 at 1-Mb resolution are shown in (A) siCtrl and (B) siAGO1 cells.

(C) Differential interaction heatmap for chromosome 2 (1Mb), showing upregulated (red) and downregulated (blue) interacting bins.

(D) Volcano plot representing differential interactions (DI) at 20-kb resolution. The upregulated interactions are shown in red and the downregulated interactions are shown in green.

(E) Venn diagrams showing the number of AGO1 ChIP-seq peaks overlapping with all differential interacting bins, at 20-kb resolution.

(F) Plot showing mean number of differential interactions calculated in 20-kb bins, based on the presence and absence of overlapping AGO1 peaks at genome-wide level (t test, p value < 0.05 and MonteCarlo permutation test (999): p value $\leq$ 0.002).

(G) Genome browser snapshot showing Hi-C interaction frequency in siCtrl (green track), siAGO1 (orange track), and AGO1 ChIP-seq peaks (blue track) at chromosome 1 locus: 12166178–117438294.

Finally, although there are differences in the numbers and size of TADs in siAGO1 cells, TAD boundaries between siCtrl and siAGO1 cells were largely maintained (Figure 6F). These results suggest that AGO1 binding at transcriptionally active enhancers contribute to the maintenance of global chromatin organization at specific genomic regions.

AGO1-Dependent Changes in 3D Genome Architecture Are Associated with Differential Gene Expression

To determine whether AGO1-dependent changes in chromatin topological structure correlated with differential gene expression, we applied an integrative approach by combining transcriptome (CAGE-seq) with Hi-C and AGO1 ChIP-seq analyses. We first examined the effect of changes in compartmentalization on gene expression. We found that in siAGO1 cells, 20% of differentially expressed genes were associated with disorganized chromatin compartments (Figures 7A–7C). Furthermore, the majority of deregulated genes that reside within topological domains, or near domain borders, overlapped with extensive changes in chromosomal interactions following AGO1 knockdown (Figure 7D). Next, all deregulated genes (FDR $\leq$ 0.05 and $\log_2$FC >1.2) located within differential interacting bins (DI bin) were further classified into two categories based on overlapping with either (1) compartment switching or (2) changes

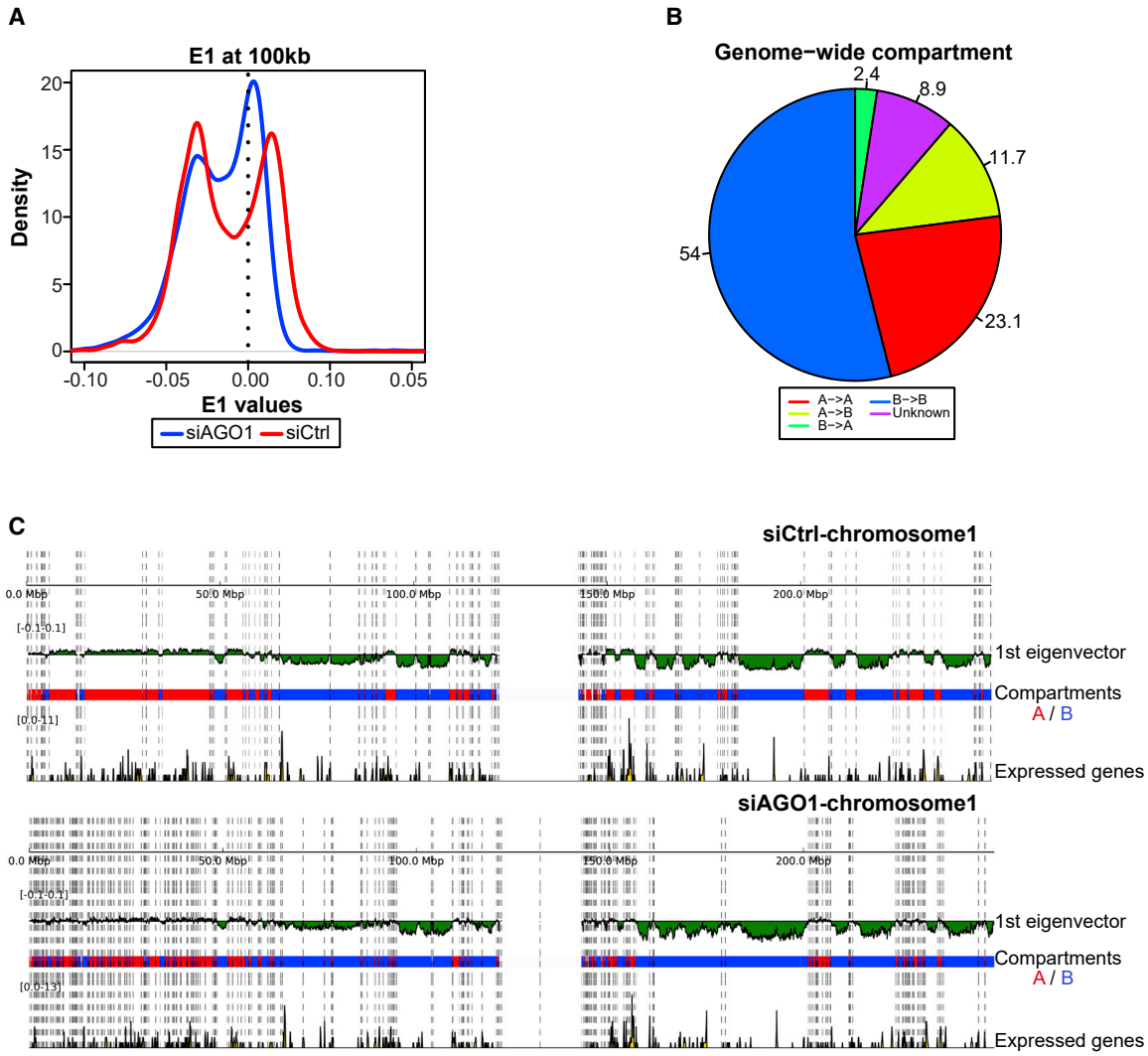

Figure 5. Changes in A/B Chromatin Compartments upon AGO1 Knockdown

(A) Density plot showing the distribution of eigenvalues of siCtrl and siAGO1 genome at 100-kb resolution. siCtrl cells followed a bimodal distribution but not the siAGO1 cells.

(B) Pie chart showing chromatin compartment changes between siCtrl and siAGO1 genomes. "A" and "B" represent open (active) and closed (inactive) compartments, respectively. "A->A" means no change in the compartment type between siCtrl and siAGO1 cells and remains "A" in both. "B->B" means no change in the compartment type between siCtrl and siAGO1 cells and remains "B" in both. "A->B" represents compartments that are A-type in siCtrl but changed to B-type in siAGO1. "B->A" represents compartments that are B-type in siCtrl but changed to A-type in siAGO1. Unknown represents when the compartment status is not known either in siCtrl or in siAGO1.

(C) First eigenvector values of chromosome 1 used to define A/B chromatin compartments, positive values represent open A-type (red) and negative values represent closed B-type (blue) compartments (top panel siCtrl and lower panel siAGO1 cells). Dotted lines delimit compartment borders. Expressed genes represent all genes identified by CAGE-seq both non-significant (genes with a basemean expression higher than 20 but not upregulated upon AGO1 knockdown) and significant genes (with a basemean expression higher than 20 and being upregulated for siAGO1 and downregulated for siCtrl cells).

in TADs configuration (Figure 7E). Furthermore, deregulated genes only from chromatin CAGE data were integrated with Hi-C changes into different categories (Figures S6A and S6B). The changes in expression of randomly selected perturbed genes (AGO1 KD CAGE-seq) located within differentially interacting bins (AGO1 KD Hi-C) were further confirmed by RT-qPCR (Figures S6C–S6F). Altogether, around 80% of deregulated genes are correlated with differential interactions (both cis- and trans interactions) (Figures 7F and 7G), and a subset of these genes is affected by compartment transitions (Figure 7A) upon AGO1 depletion. These results suggest a role for enhancer-associated AGO1 in maintaining proper transcriptional program by contributing to chromatin topological organization.

DISCUSSION

It has now become evident that AGO1 is present inside the nuclei of mammalian cells and affects multiple nuclear processes, including transcription and splicing. In this work, we report a

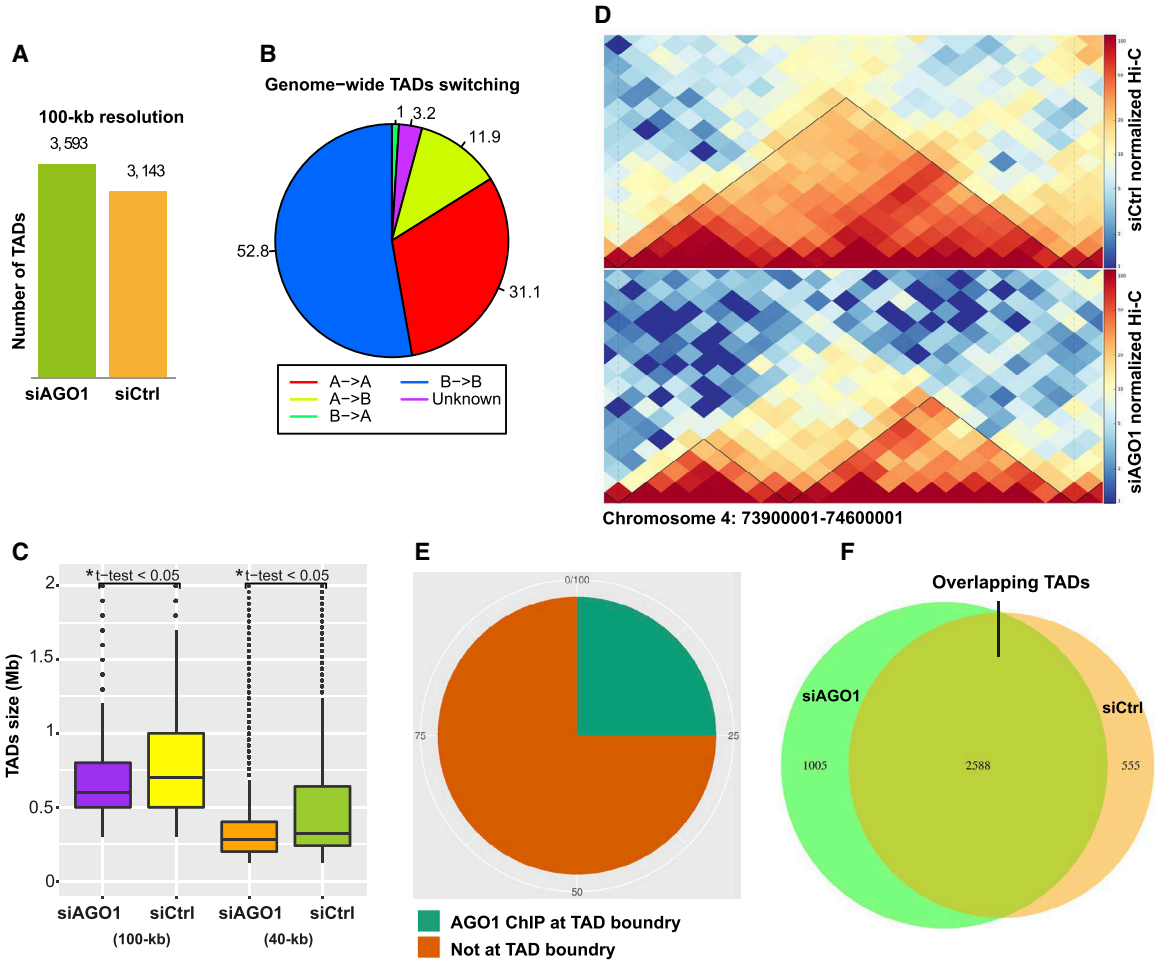

Figure 6. AGO1 Depletion Affects TADs Configuration in AGO1-Associated Regions

(A) Number of TADs identified in siCtrl and siAGO1 cells at 40-kb resolution.

(B) Pie chart showing TADs switching between A/B compartments. "A->A" and "B->B" means no switching of TADs, they remain in the same "A" and "B" compartments, respectively. "A->B" represents TADs switching from A-type in siCtrl to B-type, and "B->A" represents TADs switching from B-type in siCtrl to A-type in siAGO1. Unknown represents when the compartment status of TAD is not known.

(C) Box plot showing average size (kb) of TADs identified in siCtrl and siAGO1 cells, at both 40-kb and 100-kb resolution (t test p value < 0.05).

(D) Visualization of normalized Hi-C interactions from siCtrl and siAGO1 cells as two-dimensional heatmaps showing TADs in both conditions. TADs found in siCtrl cells are often subdivided into two or more TADs in siAGO1 cells. An example from chromosome 4 (locus: 73900001–74600001) is shown.

(E) Pie chart showing the percentage of AGO1 ChIP-seq peaks localized at TAD boundaries or not.

(F) Venn diagram showing the number of overlapping TAD boundaries between siCtrl and siAGO1 cells.

link between enhancer-associated AGO1, higher-order chromatin organization, and gene expression regulation.

In humans, there are four AGO proteins (AGO1-4) (Sasaki et al., 2003), in which only AGO2 and AGO3 possess slicer activity (Meister et al., 2004; Park et al., 2017). Unlike AGO4, which is mainly germline associated (Modzelewski et al., 2012), the non-catalytic AGO1 is broadly expressed in many tissues. Currently, it is unclear whether different AGO proteins (AGO1-4) might play a similar function in the nucleus. AGO1 depletion appears to increase AGO2 nuclear levels and also affect the nuclear redistribution of other RNAi factors (Matsui et al., 2015). Our data show that compared to AGO2-4, AGO1 proteins mostly enrich in the chromatin fractions. Also, AGO1 and AGO2 have been shown to display differential nuclear localization, with AGO1 being present in the nuclear interior and AGO2 only at the periphery (Huang et al., 2013). Unlike AGO1, AGO2 ChIP-seq analysis does not detect widespread genomic distribution (Huang et al., 2013). Notably, a recent study (van Eijl et al., 2017) reported about the cross-reactivity of another AGO2 antibody (11A9) with SMARCC1. The same antibody was previously used for ChIP (Ameyar-Zazoua et al., 2012) and protein immunoprecipitation (SWI/SNF) (Carissimi et al., 2015). Though AGO2 appears to be slightly present in chromatin fraction (as detected by western blot), its nuclear function and the genome-wide association remains unclear. Any direct or indirect mechanistic evidence that AGO2/3 would compensate for AGO1 nuclear function remains to be reported.

However, the absence of a functional slicing domain in AGO1 protein indicates its nuclear function to be independent of RNA-processing, but instead, involves RNA binding, mostly ncRNA.

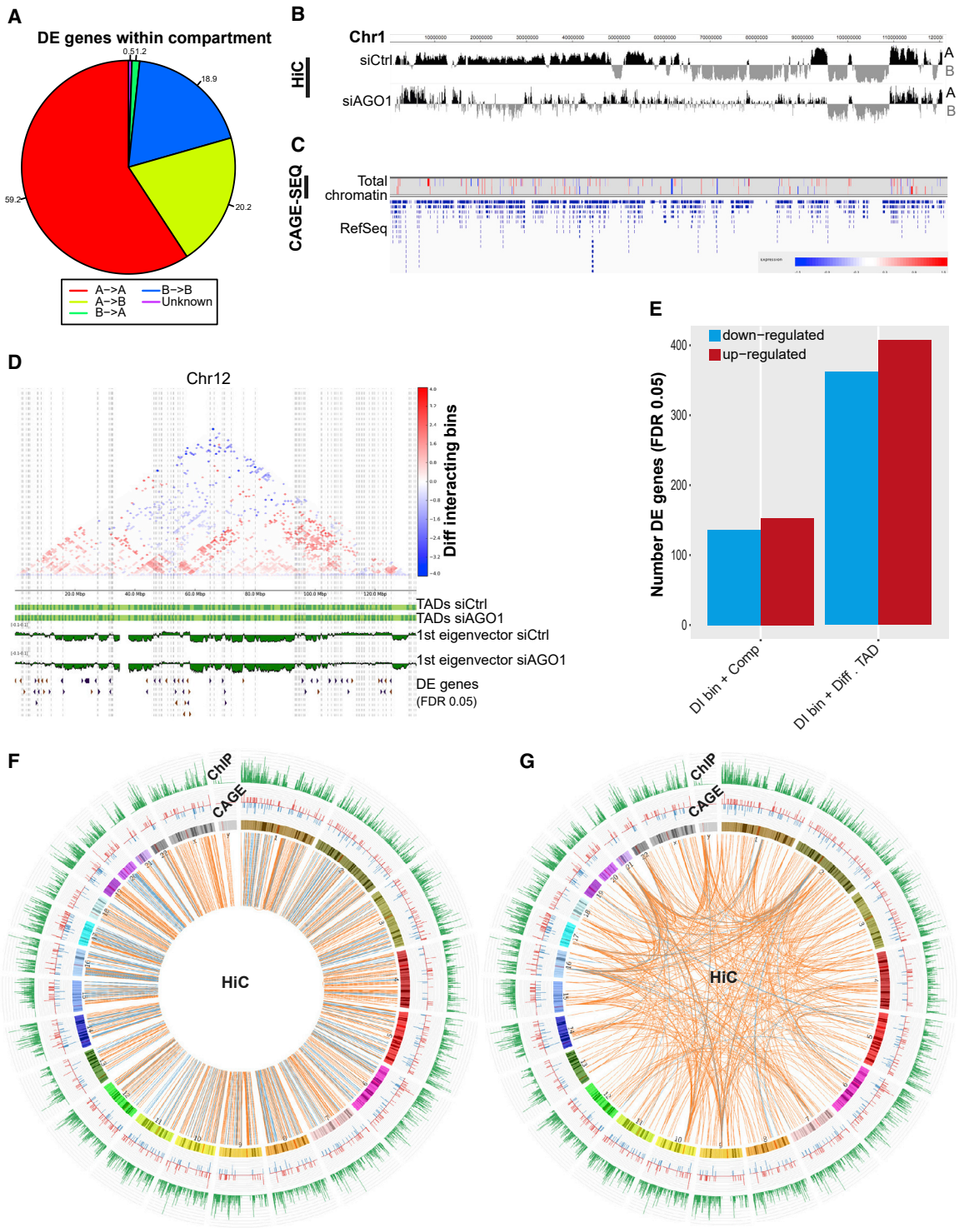

Figure 7. AGO1-Dependent Changes in 3D Genome Architecture Are Linked with Differential Gene Expression

(A) Pie chart represents distribution of all differentially expressed (DE) genes (CAGE-seq) in A/B compartments between siCtrl and siAGO1 cells. "A→A" and "B->B" represent DE genes that remain in the same "A" or "B" compartments, respectively. "A->B" represents DE genes that switched from "A" to "B" compartment and "B->A" represents DE genes that switched from "B" to "A" compartment in siAGO1 cells.

(B) Visualization of chromatin compartments A/B showing changes between siCtrl and siAGO1 cells (chromosome 1).

(C) Genome browser snapshot showing differentially expressed genes in the same region of chromosome 1 as in (B), upregulated in red and downregulated in blue (threshold FDR 0.05).

(legend continued on next page)

The mechanistic explanation of the impact of AGO1 depletion on higher-order chromatin organization remains to be understood. The role of RNA as an essential component of nuclear structure has been recognized for a long time (Nickerson et al., 1989; Holmes et al., 1972). Emerging evidence in the field of 3D genome architecture highlights the involvement of non-coding RNAs (ncRNA) in this process (Melé and Rinn, 2016; Yang et al., 2013; Cerase et al., 2015; Hacisuleyman et al., 2014). Our RIP-seq analysis in HepG2 cells identified a plethora of ncRNA moieties that are associated with chromatin-bound AGO1 and overlapped with its binding sites across the genome. Therefore, we anticipate that the RNA targets coordinating in AGO1 nuclear function are more than one. Genome-wide binding of AGO1 at transcriptionally active enhancers may suggest its role in shaping chromatin structure and gene expression by coordinating with ncRNAs, particularly eRNAs. Enhancer regions are often transcribed in a bidirectional manner by RNA polymerase II and produce eRNAs (Kim et al., 2010). The eRNAs have been shown to be involved in gene regulation by different mechanism such as controlling enhancer looping interactions (Hsieh et al., 2014; Hah et al., 2011), chromatin accessibility (Mousavi et al., 2013), and their direct interaction with CBP control enhancer activity and transcription (Bose et al., 2017). AGO1 has been shown to interact with RNA pol II across active enhancers (Huang et al., 2013; Alló et al., 2014) and may be required for eRNAs transcription. Indeed, upon AGO1 depletion, we observed obvious changes in the expression level of CAGE-defined eRNAs. These CAGE-identified eRNAs are produced from AGO1-bound enhancer regions. Moreover, the enrichment of AGO1 at active cis-regulatory elements depends on eRNAs expression, suggesting eRNAs function as a potential bridge between AGO1, chromatin association, and gene expression. AGO1, in association with eRNAs might control enhancer activity that could contribute to higher-order chromatin organization. AGO1, being a strong RNA binding protein, may play a role in establishing protein-RNA networks inside the nucleus that are essential for the stability of cell type-specific gene expression programs. Future work will, therefore, be required to investigate the mechanistic functional link between enhancer-associated AGO1 and eRNAs in the control of 3D genome organization and gene expression homeostasis.

STAR★METHODS

Detailed methods are provided in the online version of this paper and include the following:

SUPPLEMENTAL INFORMATION

Supplemental Information can be found online at https://doi.org/10.1016/j.cels.2019.09.005.

ACKNOWLEDGMENTS

We are grateful to Hakan Ozadam and Johan Gibcus from Job Dekker group (University of Massachusetts Medical School, USA) for initial help in calling Hi-C interactions, Riccardo Aiese Cigliano (Sequentia Biotech) for bioinformatic analysis, and Heno Hwang (scientific illustrator) at King Abdullah University of Science and Technology (KAUST) for his help in drawing the graphical abstract. This work was supported by EPIGEN-CNR (Italian Ministry of University and Research) and King Abdullah University of Science and Technology (KAUST) to V.O.

AUTHOR CONTRIBUTIONS

M.S. conceived this study, designed and performed experiments, analyzed the data, and wrote the manuscript with input from all the authors. K.M.P. conceived this study, designed, performed experiments, and analyzed the data. S.A.A. with M.S. performed Hi-C experiments. M.T. and H.K. performed computational analyses of CAGE-seq and ChIP-seq data. L.S. and T.R. performed computational analyses of ChIP-seq and CAGE-seq data integration. Y.G. performed computational analyses of RIP-seq and ChIP-seq integration. A.F. contributed in RIP-seq experiments. B.F. helped in western blotting. P.C. and H.K. produced and analyzed the CAGE-seq experiment. V.O. conceived this study, designed experiments, and wrote the manuscript.

(D) A representative plot of chromosome 12 showing (1) differential interactions up-interacting bins (red) and down-interacting bins (blue), (2) TADs configuration in siCtrl and siAGO1 cells (100-kb resolution), and (3) compartments in siCtrl and siAGO, and (4) differentially expressed genes with upregulated in purple and downregulated in brown (threshold FDR 0.05). The vertical dotted lines reflect compartment switching between siCtrl and siAGO1 cells.
(E) Bar plot showing classification of differentially expressed genes into two categories based on integration with AGO1 ChIP-seq and Hi-C data. This plot contains the number of DE genes (FDR threshold 0.05) overlapping with AGO1-bound differentially interacting bins that either associate with different TADs configuration (DI bin + Diff.TAD), and/or compartment switching (DI bin + Comp) between siCtrl and siAGO1 cells.
(F and G) CIRCOS plot illustrating the position of significant intra- (F) and inter- (G) chromosomal differential interactions (FDR < 0.001 and logFC > 3), down-interacting regions are linked by blue lines while the up-interacting bins are linked by orange lines. The three circles in the plot represent the following data; 1.Chromosome names, 2.DE genes (FDR 0.05; upregulated genes [red] downregulated genes [blue]), 3.AGO1 ChIP-seq peaks (green).

DECLARATION OF INTERESTS

The authors declare no competing interests.

Received: April 1, 2019
Revised: July 29, 2019
Accepted: September 12, 2019
Published: October 16, 2019

REFERENCES

Agirre, E., Bellora, N., Alló, M., Pagès, A., Bertucci, P., Kornblihtt, A.R., and Eyras, E. (2015). A chromatin code for alternative splicing involving a putative association between CTCF and HP1alpha proteins. BMC Biol. *13*, 31.

Alló, M., Agirre, E., Bessonov, S., Bertucci, P., Gómez Acuña, L., Buggiano, V., Bellora, N., Singh, B., Petrillo, E., Blaustein, M., et al. (2014). Argonaute-1 binds transcriptional enhancers and controls constitutive and alternative splicing in human cells. Proc. Natl. Acad. Sci. USA *111*, 15622–15629.

Ameyar-Zazoua, M., Rachez, C., Souidi, M., Robin, P., Fritsch, L., Young, R., Morozova, N., Fenouil, R., Descostes, N., Andrau, J.C., et al. (2012). Argonaute proteins couple chromatin silencing to alternative splicing. Nat. Struct. Mol. Biol. *19*, 998–1004.

Andersson, R., Gebhard, C., Miguel-Escalada, I., Hoof, I., Bornholdt, J., Boyd, M., Chen, Y., Zhao, X., Schmidl, C., Suzuki, T., et al. (2014). An atlas of active enhancers across human cell types and tissues. Nature *507*, 455–461.

Ashoor, H., Hérault, A., Kamoun, A., Radvanyi, F., Bajic, V.B., Barillot, E., and Boeva, V. (2013). HMCan: a method for detecting chromatin modifications in cancer samples using ChIP-seq data. Bioinformatics *29*, 2979–2986.

Babicki, S., Arndt, D., Marcu, A., Liang, Y.J., Grant, J.R., Maciejewski, A., and Wishart, D.S. (2016). Heatmapper: web-enabled heat mapping for all. Nucleic Acids Res. *44*, W147–W153.

Belton, J.M., Mccord, R.P., Gibcus, J.H., Naumova, N., Zhan, Y., and Dekker, J. (2012). Hi-C: a comprehensive technique to capture the conformation of genomes. Methods *58*, 268–276.

Bose, D.A., Donahue, G., Reinberg, D., Shiekhattar, R., Bonasio, R., and Berger, S.L. (2017). RNA binding to CBP stimulates histone acetylation and transcription. Cell *168*, 135–149.

Bouvy-Liivrand, M., Hernández de Sande, A., Pölönen, P., Mehtonen, J., Vuorenmaa, T., Niskanen, H., Sinkkonen, L., Kaikkonen, M.U., and Heinäniemi, M. (2017). Analysis of primary microRNA loci from nascent transcriptomes reveals regulatory domains governed by chromatin architecture. Nucleic Acids Res. *45*, 12054.

Bouwman, B.A., and de Laat, W. (2015). Getting the genome in shape: the formation of loops, domains and compartments. Genome Biol. *16*, 154.

Bulger, M., and Groudine, M. (2011). Functional and mechanistic diversity of distal transcription enhancers. Cell *144*, 825.

Carissimi, C., Laudadio, I., Cipolletta, E., Gioiosa, S., Mihailovich, M., Bonaldi, T., Macino, G., and Fulci, V. (2015). ARGONAUTE2 cooperates with SWI/SNF complex to determine nucleosome occupancy at human transcription start sites. Nucleic Acids Res. *43*, 1498–1512.

Cerase, A., Pintacuda, G., Tattermusch, A., and Avner, P. (2015). Xist localization and function: new insights from multiple levels. Genome Biol. *16*, 166.

Cernilogar, F.M., Onorati, M.C., Kothe, G.O., Burroughs, A.M., Parsi, K.M., Breiling, A., Lo Sardo, F., Saxena, A., Miyoshi, K., Siomi, H., et al. (2011). Chromatin-associated RNA interference components contribute to transcriptional regulation in Drosophila. Nature *480*, 391–395.

Chou, C.H., Shrestha, S., Yang, C.D., Chang, N.W., Lin, Y.L., Liao, K.W., Huang, W.C., Sun, T.H., Tu, S.J., Lee, W.H., et al. (2018). miRTarBase update 2018: a resource for experimentally validated microRNA-target interactions. Nucleic Acids Res. *46*, D296–D302.

Delest, A., Sexton, T., and Cavalli, G. (2012). Polycomb: a paradigm for genome organization from one to three dimensions. Curr. Opin. Cell Biol. *24*, 405–414.

Dixon, J.R., Selvaraj, S., Yue, F., Kim, A., Li, Y., Shen, Y., Hu, M., Liu, J.S., and Ren, B. (2012). Topological domains in mammalian genomes identified by analysis of chromatin interactions. Nature *485*, 376–380.

Hacisuleyman, E., Goff, L.A., Trapnell, C., Williams, A., Henao-Mejia, J., Sun, L., Mcclanahan, P., Hendrickson, D.G., Sauvageau, M., Kelley, D.R., et al. (2014). Topological organization of multichromosomal regions by the long intergenic noncoding RNA Firre. Nat. Struct. Mol. Biol. *21*, 198–206.

Hah, N., Danko, C.G., Core, L., Waterfall, J.J., Siepel, A., Lis, J.T., and Kraus, W.L. (2011). A rapid, extensive, and transient transcriptional response to estrogen signaling in breast cancer cells. Cell *145*, 622–634.

Hah, N., Murakami, S., Nagari, A., Danko, C.G., and Kraus, W.L. (2013). Enhancer transcripts mark active estrogen receptor binding sites. Genome Res. *23*, 1210–1223.

Harrow, J., Frankish, A., Gonzalez, J.M., Tapanari, E., Diekhans, M., Kokocinski, F., Aken, B.L., Barrell, D., Zadissa, A., Searle, S., et al. (2012). GENCODE: the reference human genome annotation for the ENCODE Project. Genome Res. *22*, 1760–1774.

Hoffman, M.M., Ernst, J., Wilder, S.P., Kundaje, A., Harris, R.S., Libbrecht, M., Giardine, B., Ellenbogen, P.M., Bilmes, J.A., Birney, E., et al. (2013). Integrative annotation of chromatin elements from ENCODE data. Nucleic Acids Res. *41*, 827–841.

Holmes, D.S., Mayfield, J.E., Sander, G., and Bonner, J. (1972). Chromosomal RNA: its properties. Science *177*, 72–74.

Hsieh, C.L., Fei, T., Chen, Y.W., Li, T.T., Gao, Y.F., Wang, X.D., Sun, T., Sweeney, C.J., Lee, G.S.M., Chen, S.Y., et al. (2014). Enhancer RNAs participate in androgen receptor-driven looping that selectively enhances gene activation. Proc. Natl. Acad. Sci. USA *111*, 7319–7324.

Huang, V., Zheng, J., Qi, Z., Wang, J., Place, R.F., Yu, J., Li, H., and Li, L.C. (2013). Ago1 Interacts with RNA polymerase II and binds to the promoters of actively transcribed genes in human cancer cells. PLoS Genet. *9*, e1003821.

Joshua-Tor, L., and Hannon, G.J. (2011). Ancestral roles of small RNAs: an Ago-centric perspective. Cold Spring Harb. Perspect. Biol. *3*, a003772.

Kagey, M.H., Newman, J.J., Bilodeau, S., Zhan, Y., Orlando, D.A., Van Berkum, N.L., Ebmeier, C.C., Goossens, J., Rahl, P.B., Levine, S.S., et al. (2010). Mediator and cohesin connect gene expression and chromatin architecture. Nature *467*, 430–435.

Kim, T.K., Hemberg, M., Gray, J.M., Costa, A.M., Bear, D.M., Wu, J., Harmin, D.A., Laptewicz, M., Barbara-Haley, K., Kuersten, S., et al. (2010). Widespread transcription at neuronal activity-regulated enhancers. Nature *465*, 182–187.

Kumar, D., Shadrach, J.L., Wagers, A.J., and Lassar, A.B. (2009). Id3 is a direct transcriptional target of Pax7 in quiescent satellite cells. Mol. Biol. Cell *20*, 3170–3177.

Langmead, B., and Salzberg, S.L. (2012). Fast gapped-read alignment with Bowtie 2. Nat. Methods *9*, 357–359.

Li, H., Handsaker, B., Wysoker, A., Fennell, T., Ruan, J., Homer, N., Marth, G., Abecasis, G., and Durbin, R.; 1000 Genome Project Data Processing Subgroup (2009). The sequence alignment/map format and SAMtools. Bioinformatics *25*, 2078–2079.

Li, Q.H., Brown, J.B., Huang, H.Y., and Bickel, P.J. (2011). Measuring reproducibility of high-throughput experiments. Ann. Appl. Stat. *5*, 1752–1779.

Lieberman-Aiden, E., Van Berkum, N.L., Williams, L., Imakaev, M., Ragoczy, T., Telling, A., Amit, I., Lajoie, B.R., Sabo, P.J., Dorschner, M.O., et al. (2009). Comprehensive mapping of long-range interactions reveals folding principles of the human genome. Science *326*, 289–293.

Lun, A.T., and Smyth, G.K. (2015). diffHic: a bioconductor package to detect differential genomic interactions in Hi-C data. BMC Bioinformatics *16*, 258.

Matsui, M., Li, L.D., Janowski, B.A., and Corey, D.R. (2015). Reduced expression of Argonaute 1, Argonaute 2, and TRBP changes levels and intracellular distribution of RNAi factors. Sci. Rep. *5*, 12855.

Meister, G. (2013). Argonaute proteins: functional insights and emerging roles. Nat. Rev. Genet. *14*, 447–459.

Meister, G., Landthaler, M., Patkaniowska, A., Dorsett, Y., Teng, G., and Tuschl, T. (2004). Human Argonaute2 mediates RNA cleavage targeted by miRNAs and siRNAs. Mol. Cell *15*, 185–197.

Melé, M., and Rinn, J.L. (2016). "Cat's Cradling' the 3D genome by the act of LncRNA transcription. Mol. Cell *62*, 657–664.

Modzelewski, A.J., Holmes, R.J., Hilz, S., Grimson, A., and Cohen, P.E. (2012). AGO4 regulates entry into meiosis and influences silencing of sex chromosomes in the male mouse germline. Dev. Cell *23*, 251–264.

Moshkovich, N., Nisha, P., Boyle, P.J., Thompson, B.A., Dale, R.K., and Lei, E.P. (2011). RNAi-independent role for Argonaute2 in CTCF/CP190 chromatin insulator function. Genes Dev. *25*, 1686–1701.

Mousavi, K., Zare, H., Dell'Orso, S., Grontved, L., Gutierrez-Cruz, G., Derfoul, A., Hager, G.L., and Sartorelli, V. (2013). eRNAs promote transcription by establishing chromatin accessibility at defined genomic loci. Mol. Cell *51*, 606–617.

Natoli, G., and Andrau, J.C. (2012). Noncoding transcription at enhancers: general principles and functional models. Annu. Rev. Genet. *46*, 1–19.

Neph, S., Kuehn, M.S., Reynolds, A.P., Haugen, E., Thurman, R.E., Johnson, A.K., Rynes, E., Maurano, M.T., Vierstra, J., Thomas, S., et al. (2012). BEDOPS: high-performance genomic feature operations. Bioinformatics *28*, 1919–1920.

Nickerson, J.A., Krochmalnic, G., Wan, K.M., and Penman, S. (1989). Chromatin architecture and nuclear-RNA. Proc. Natl. Acad. Sci. USA *86*, 177–181.

Nora, E.P., Lajoie, B.R., Schulz, E.G., Giorgetti, L., Okamoto, I., Servant, N., Piolot, T., Van Berkum, N.L., Meisig, J., Sedat, J., et al. (2012). Spatial partitioning of the regulatory landscape of the X-inactivation centre. Nature *485*, 381–385.

Ong, C.T., and Corces, V.G. (2011). Enhancer function: new insights into the regulation of tissue-specific gene expression. Nat. Rev. Genet. *12*, 283–293.

Park, M.S., Phan, H.D., Busch, F., Hinckley, S.H., Brackbill, J.A., Wysocki, V.H., and Nakanishi, K. (2017). Human Argonaute3 has slicer activity. Nucleic Acids Res. *45*, 11867–11877.

Pohl, A., and Beato, M. (2014). bwtool: a tool for bigWig files. Bioinformatics *30*, 1618–1619.

Quinlan, A.R., and Hall, I.M. (2010). BEDTools: a flexible suite of utilities for comparing genomic features. Bioinformatics *26*, 841–842.

Rahman, R.U., Gautam, A., Bethune, J., Sattar, A., Fiosins, M., Magruder, D.S., Capece, V., Shomroni, O., and Bonn, S. (2018). Oasis 2: improved online analysis of small RNA-seq data. BMC Bioinformatics *19*, 54.

Rao, S.S.P., Huntley, M.H., Durand, N.C., Stamenova, E.K., Bochkov, I.D., Robinson, J.T., Sanborn, A.L., Machol, I., Omer, A.D., Lander, E.S., et al. (2014). A 3D map of the human genome at kilobase resolution reveals principles of chromatin looping. Cell *159*, 1665–1680.

Salimullah, M., Sakai, M., Plessy, C., and Carninci, P. (2011). NanoCAGE: a high-resolution technique to discover and interrogate cell transcriptomes. Cold Spring Harb. Protoc. *2011*, pdb.prot5559.

Sasaki, T., Shiohama, A., Minoshima, S., and Shimizu, N. (2003). Identification of eight members of the Argonaute family in the human genome. Genomics *82*, 323–330.

Schoenfelder, S., Furlan-Magaril, M., Mifsud, B., Tavares-Cadete, F., Sugar, R., Javierre, B.M., Nagano, T., Katsman, Y., Sakthidevi, M., Wingett, S.W., et al. (2015). The pluripotent regulatory circuitry connecting promoters to their long-range interacting elements. Genome Res. *25*, 582–597.

Seitan, V.C., Faure, A.J., Zhan, Y., Mccord, R.P., Lajoie, B.R., Ing-Simmons, E., Lenhard, B., Giorgetti, L., Heard, E., Fisher, A.G., et al. (2013). Cohesin-based chromatin interactions enable regulated gene expression within preexisting architectural compartments. Genome Res. *23*, 2066–2077.

Serra, F., Baù, D., Filion, G., and Marti-Renom, M.A. (2016). Structural features of the fly chromatin colors revealed by automatic three-dimensional modeling. bioRxiv. https://doi.org/10.1101/036764.

Serra, F., Baù, D., Goodstadt, M., Castillo, D., Filion, G.J., and Marti-Renom, M.A. (2017). Automatic analysis and 3D-modelling of Hi-C data using TADbit reveals structural features of the fly chromatin colors. PLoS Comput. Biol. *13*, e1005665.

Servant, N., Varoquaux, N., Lajoie, B.R., Viara, E., Chen, C.J., Vert, J.P., Heard, E., Dekker, J., and Barillot, E. (2015). HiC-Pro: an optimized and flexible pipeline for Hi-C data processing. Genome Biol. *16*, 259.

Sofueva, S., Yaffe, E., Chan, W.C., Georgopoulou, D., Vietri Rudan, M., Mira-Bontenbal, H., Pollard, S.M., Schroth, G.P., Tanay, A., and Hadjur, S. (2013). Cohesin-mediated interactions organize chromosomal domain architecture. EMBO J. *32*, 3119–3129.

Takahashi, H., Lassmann, T., Murata, M., and Carninci, P. (2012). 5′ End-centered expression profiling using cap-analysis gene expression and next-generation sequencing. Nat. Protoc. *7*, 542–561.

Uren, P.J., Bahrami-Samani, E., Burns, S.C., Qiao, M., Karginov, F.V., Hodges, E., Hannon, G.J., Sanford, J.R., Penalva, L.O.F., and Smith, A.D. (2012). Site identification in high-throughput RNA-protein interaction data. Bioinformatics *28*, 3013–3020.

van Eijl, R.A.P.M., Van Den Brand, T., Nguyen, L.N., and Mulder, K.W. (2017). Reactivity of human AGO2 monoclonal antibody 11A9 with the SWI/SNF complex: a case study for rigorously defining antibody selectivity. Sci. Rep. *7*, 7278.

Volpe, T.A., Kidner, C., Hall, I.M., Teng, G., Grewal, S.I., and Martienssen, R.A. (2002). Regulation of heterochromatic silencing and histone H3 lysine-9 methylation by RNAi. Science *297*, 1833–1837.

Yang, L.Q., Lin, C.R., Jin, C.Y., Yang, J.C., Tanasa, B., Li, W.B., Merkurjev, D., Ohgi, K.A., Meng, D., Zhang, J., et al. (2013). lncRNA-dependent mechanisms of androgen-receptor-regulated gene activation programs. Nature *500*, 598–602.

Zhang, Y., Mccord, R.P., Ho, Y.J., Lajoie, B.R., Hildebrand, D.G., Simon, A.C., Becker, M.S., Alt, F.W., and Dekker, J. (2012). Spatial organization of the mouse genome and its role in recurrent chromosomal translocations. Cell *148*, 908–921.

Zilberman, D., Cao, X., and Jacobsen, S.E. (2003). ARGONAUTE4 control of locus-specific siRNA accumulation and DNA and histone methylation. Science *299*, 716–719.

Zuin, J., Dixon, J.R., Van Der Reijden, M.I., Ye, Z., Kolovos, P., Brouwer, R.W., Van De Corput, M.P., Van De Werken, H.J., Knoch, T.A., van IJcken, W.F., et al. (2014). Cohesin and CTCF differentially affect chromatin architecture and gene expression in human cells. Proc. Natl. Acad. Sci. USA *111*, 996–1001.

STAR★METHODS

KEY RESOURCES TABLE

REAGENT or RESOURCE	SOURCE	IDENTIFIER
Antibodies		
Mouse monoclonal anti-AGO1 (Clone#2A7)	Wako	015-22411; RRID: AB_2096179
Mouse monoclonal anti-AGO1 sup	Gift (Mikiko Siomi)	N/A
Rabbit Anti-Argonaute 2 Monoclonal Antibody (Clone C34C6)	Cell Signaling Technology	2897; RRID: AB_2096291
Argonaute 3 (D15D2) Rabbit mAb antibody	Cell Signaling Technology	5054; RRID: AB_2797607
Argonaute 4 (D10F10) Rabbit mAb antibody	Cell Signaling Technology	6913; RRID: AB_10828811
β-Tubulin antibody	Cell Signaling Technology	Cat# 2146; RRID: AB_2210545
Histone H3 antibody	Cell Signaling Technology	Cat# 9715; RRID: AB_331563
HA tag antibody - ChIP Grade	Abcam	ab9110; RRID: AB_307019
Alexa flour 647	Abcam	Cat# ab150115; RRID: AB_2687948
Chemicals, Peptides, and Recombinant Proteins		
Protein G Dynabeads	ThermoFisher	10003D
Ampure XP paramagnetic beads	Beckman Coulter	A63881
Complete Mini EDTA-free proteinase inhibitor	Roche	11836170001
HindIII	New England Biolabs	R0104S
T4 DNA ligase	New England Biolabs	M0202S
Dynabeads M-280 streptavidin	ThermoFisher	11206D
Biotin-14-dATP	ThermoFisher	19524016
RNase A	Thermo Fisher	EN0531
RNase A/T1 Mix	Thermo Fisher	EN0551
Proteinase K	New England Biolabs	P8107S
TRIzol reagent	Thermo Fisher	15596026
AlamarBlue Dye	Thermo Fisher	DAL1025
Critical Commercial Assays		
ChIP DNA Clean & Concentrator	Zymo Research	D5205
QuantiTect Reverse Transcription Kit	Qiagen	205311
Direct-zol RNA Miniprep	Zymo Research	R2050
Qubit dsDNA HS Assay Kit	ThermoFisher	Q32854
Qubit RNA HS Assay Kit	ThermoFisher	Q32852
TruSeq Small RNA Library Prep Kit	Illumina	RS-200-0012
TruSeq Stranded Total RNA Library Prep	Illumina	20020596
TruSeq ChIP Library Preparation Kit	Illumina	IP-202-1012
Deposited Data		
CAGE-seq (Chromatin and Total RNA in siCtrl, siAGO1 and control HepG2 cells)	This study	SRA: PRJNA398595
AGO1 ChIP-seq (HepG2)	This study	SRA: PRJNA398595
Small RNA-seq (siCtrl and siAGO1 HepG2 cells)	This study	SRA: PRJNA398595
Hi-C-seq (siCtrl and siAGO1 HepG2 cells)	This study	SRA: PRJNA398595
AGO1 RIP-seq (HepG2)	This study	SRA: PRJNA543746
AGO1 and HA-AGO1 comparison-test ChIP-seq	This study	SRA: PRJNA543746
GRO-seq (HepG2)	(Bouvy-Liivrand et al., 2017)	GEO: GSE92375

(*Continued on next page*)

Continued

REAGENT or RESOURCE	SOURCE	IDENTIFIER
H3K27ac, H3K4me1, H3K4me3, and H3K9ac ChIP-seq (HepG2)	https://www.encodeproject.org/	GEO: GSE29611
Chromatin segmentations (HepG2)	(Hoffman et al., 2013)	ENCODE Genome Segmentation
Experimental Models: Cell Lines		
HepG2	ATCC	HB-8065
HEK 293T	ATCC	CRL-3216
Oligonucleotides		
Oligo DNA primers for RT-qPCR, ChIP-qPCR, and siRNA information	Table S5	N/A
Recombinant DNA		
Plasmid: pOZ-FH-C-puro, retroviral vector (Used for expressing HA-FLAG-tagged AGO1)	A kind gift from Andrew Lassar (Kumar et al., 2009)	Addgene plasmid # 32516, RRID: Addgene_32516
Software and Algorithms		
Small RNA-seq analysis tool Oasis 2.0	(Rahman et al., 2018)	https://oasis.dzne.de
mirTarBase tool	(Chou et al., 2018)	mirtarbase.mbc.nctu.edu.tw/php/
Cutadapt 1.12	(https://github.com/marcelm/cutadapt/	https://github.com/marcelm/cutadapt/
R package CAGEr	https://bioconductor.org/packages/release/bioc/html/CAGEr.html	https://bioconductor.org/packages/release/bioc/html/CAGEr.html
Bioconductor package DESeq2	https://bioconductor.org/packages/release/bioc/html/DESeq2.html	https://bioconductor.org/packages/release/bioc/html/DESeq2.html
Sickle	http://www.citeulike.org/user/mvermaat/article/13260426	http://www.citeulike.org/user/mvermaat/article/13260426
Bowtie	(Langmead and Salzberg, 2012)	Version 2.2.5
Samtools	(Li et al., 2009)	Version 1.2
HMCan peak calling tool	(Ashoor et al., 2013)	N/A
Irreproducibility Discovery Rate (IDR) analysis	(Li et al., 2011)	N/A
Bedtools	(Quinlan and Hall, 2010)	N/A
BEDOPS	(Neph et al., 2012)	N/A
bwtools	(Pohl and Beato, 2014)	Version 2.17
HiC-Pro pipeline	(Servant et al., 2015)	Version 2.7.8
R package diffHiC	(Lun and Smyth, 2015)	Version 1.6.0
TADbit	(Serra et al., 2017)	Version 0.2.0.23
HiCExplorer	http://hicexplorer.readthedocs.io/en/latest/index.html	Version 1.3
Piranha	(Uren et al., 2012)	Version 1.2.1
Heatmapper	(Babicki et al., 2016)	N/A
Other		
GENCODE v19	GENCODE (Harrow et al., 2012)	https://www.gencodegenes.org/releases/19.html

LEAD CONTACT AND MATERIALS AVAILABILITY

Further information and requests for resources should be directed to and will be fulfilled by the Lead Contact (valerio.orlando@kaust.edu.sa). This study did not generate new unique reagents.

EXPERIMENTAL MODEL AND SUBJECT DETAILS

Cell Lines

HepG2 (ATCC, HB-8065, male) and HEK-293 (ATCC, CRL-3216, female) cells were purchased from ATCC before experiments and thus considered authenticated.

METHOD DETAILS

Cell Culture and Transfection

HepG2 and HEK-293 cells were cultured in EMEM medium (Sigma, Cat # M0643) supplemented with 10% FBS (Invitrogen, Cat # 26140-079) 1% penicillin and streptomycin (Euroclone, Cat # ECB3001D). Cell culture was maintained at 37°C and 5% CO2. HepG2 cells were transiently transfected with a pool of four siRNAs against AGO1 (FlexiTube GeneSolution GS26523, cat# SI00377454, SI00377447, SI00377440, and SI00377433) by using HiPerfect reagent (Qiagen). After 48hrs of incubation, cells were harvested for further analysis. Cell viability was assessed using alamarBlue cell viability reagent (Cat# DAL1025) according to the manufacture's instructions. For flow cytometry, cells were pelleted and fixed in ice cold 70% ethanol. After fixation the cell pellet was resuspended in the PI staining solution (0.1% Triton X-100, 10 μg/mL propidium iodide and 100 μg/mL RNase A). Cell-cycle analysis was performed using BD FACSCanto II system and experiments were repeated three times.

Antibodies

Mouse monoclonal anti-AGO1 sup (Mikiko Siomi) anti-AGO1 (clone 2A7, Wako), β-tubulin antibody (#2146, Cell Signaling), and rabbit monoclonal histone H3 antibody (#9715, Cell Signaling), anti-AGO-2 (#2897 Cell Signaling), anti-AGO3 (#5054 Cell Signaling), and anti-AGO4 (#6913 Cell Signaling) were used as primary antibody for western blotting or immunofluorescence. Alexa flour 647 Goat anti-mouse IgG (H+L) (ab150115, Abcam) was used as secondary antibody for immunofluorescence. Mouse monoclonal anti-AGO1 (clone 2A7, Wako) and rabbit polyclonal HA-tag antibody (Abcam, # ab9110) for ChIP experiment. Anti-AGO1 (clone 2A7, Wako) was used for control validation by ChIP-qPCR, western blot, and immunofluorescence.

Chromatin Fractionation and Western Blot

Cells were lysed in RIPA buffer (10 mM Tris pH 8.0, 1 mM EDTA, 0.5 mM EGTA, 1% Triton X-100, 0.1% Sodium deoxycholate, 0.1% SDS, 150 mM EDTA and 0.5 mM PMSF, 10 U/ml Superase-In, 1X Protease inhibitor cocktail), incubated for 30 minutes on ice, and spun at 13000 rpm for 10 min to collect supernatant as total fraction (T). For chromatin fractionation, cells were lysed in CSKI buffer (10 mM Pipes pH 6.8, 100 mM NaCl, 1 mM EDTA, 300 mM Sucrose, 1 mM MgCl2, 1 mM DTT, 0.5% Triton X-100, 10 U/ml Superase-In, 1X Protease inhibitor cocktail) for 15 min on ice (vortexed occasionally) and spun at 3000 rpm for 5 min to remove the soluble fraction (S). Pellet was resuspended in CSK II buffer (10 mM Pipes pH 6.8, 50 mM NaCl, 300 mM Sucrose, 6 mM $MgCl_2$, 1mM DTT), treated with DNase I (Promega, M610A) for 25 min at 30°C, and followed by extraction with 250 mM $(NH_4)_2SO_4$ for 10 min. The extract was centrifuged at 1200g for 10 min at 4°C to collect the supernatant as chromatin bound fraction (CB). Protein samples from all fractions were denatured in 1X Laemmli buffer (100mM DTT) and separated on 4-12% gradient Bis-Tris gels (NuPAGE), and then transferred onto a nitrocellulose membrane (GE Healthcare) for 2 hours. The membrane was blocked with 5% milk in PBST, incubated in primary antibody overnight, washed with PBST, and incubated with secondary antibody for 1 hour. Western-blot signals were visualized using ECL Reagent (Amersham) and ChemiDoc Imaging System (Bio-Rad).

For chromatin association assay in the presence of RNAse, the pellet obtained after soluble fraction (S) was divided into two fractions. The first half fraction was treated with 15ul of RNaseA/T1 (Ambion, AM2275); the other half was treated with same volume of RNase storage buffer (50mM Tris pH 7.4, 300mM NaCl, 0.5% NP-40, 1mM EDTA) at room temperature for 30 minutes and then followed the chromatin extraction steps as mentioned above. Band intensities from two independent chromatin fractionation assays were quantified using Image Lab software (ChemiDoc, BioRad).

Immunofluorescence

HepG2 cells were fixed with 4% formaldeyhyde for AGO1 staining. Immunofluorescence was performed according to standard procedure. Images were acquired by using confocal microscope (Zeiss).

nanoCAGE-seq

After cellular fractionation of HepG2 cells as described above, the total and chromatin bound fraction samples were added with Trizol for RNA extraction. The RNA purification was performed with Direct-zol RNA Miniprep kit (ZymoResearch) and then quantified by quibit (Qubit RNA HS Assay Kit). Samples were processed for nanoCAGEseq as described earlier (Salimullah et al., 2011).

ChIP-seq

HepG2 cells were cross-linked with 2% formaldehyde on shaking platform for 12 min at room temperature. The reaction was quenched with 125 mM of glycine, and cells were collected by scraping. The pellet was further processed by incubating in lysis buffer (5 mM HEPES/KOH pH 8.0, 85 mM KCl, 0.5% NP-40, 0.5 mM PMSF) for 30 min on ice. Pelleted nuclei were resuspended in shearing buffer (50 mM Tris/HCl pH 8.0, 1 mM EDTA, 0.1% SDS, 0.5% DOC, 0.5 mM PMSF), passed through 1 ml syringe for 10-15 times, and sonicated with Diagenode Bioruptor (total 3 cycles for 7 min each with settings 30 sec ON and 30 sec OFF at maximum amplitude). To remove debris, sonicated samples were spun at 16000xg for 20 min at 4°C. Supernatant was collected and chromatin DNA fragment size (average 500 bp) was checked after decrosslinking at 65°C for 4 hrs on 2% agarose gel. Chromatin suspension was mixed with 1X IP buffer (1 mM Tris/HCl pH 7.4, 0.1 mM EDTA, 0.1% Triton X-100, 0.05% DOC and 150 mM NaCl, 0.5 mM PMSF), AGO1 antibody (Wako, Clone 2A7) and rotated overnight on a rocker wheel at 4oC. Immuno-complexes were captured with Dyna beads Protein G (Invitrogen) for 2 hrs on a rocker wheel at 4°C. Further, beads were washed with 2X Low Salt buffer (20 mM Tris/HCl pH 8.0, 2 mM

EDTA, 0.1% SDS, 1% Triton X-100, 150 mM NaCl, 0.5 mM PMSF), 2X High Salt buffer (20 mM Tris/HCl pH 8.0, 2 mM EDTA, 0.1% SDS, 1% Triton X-100, 500 mM NaCl, 0.5 mM PMSF), 1X LiCl buffer (10 mM Tris/HCl pH8.0, 10 mM EDTA, 1% NP-40, 250 mM LiCl, 0.5 mM PMSF), and 1X TE (1 mM Tris/HCl pH 8.0, 1 mM EDTA). Finally, immunocomplexes were eluted (1 mM Tris/HCl pH 8.0, 10 mM EDTA, 1% SDS) at 65°C for 20 min, cross-links were reversed at 65°C overnight, treated with RNase A, proteinase K and then DNA was extracted with Phenol:Chloroform:Isoamyl alcohol (25:24:1). The extracted ChIP-DNA (using ChIP-DNA Clean & Concentrator, Zymo) was processed for high-throughput library preparation (TruSeq ChIP Library Preparation Kit, illumina). The ChIP libraries were purified using Ampure XP beads and were quantified using qubit dsDNA HS assay kit.

For ChIP experiment after actinomycin D treatment. HepG2 cells were treated with actinomycin D (1.6 μM) or DMSO (as a control) for 6 hour before collecting for fixation.

Stable FLAG- HA-tagged AGO1 HepG2 Cell Lines

Stable HepG2 cell lines expressing AGO1 proteins fused to C-terminal FLAG and HA epitope tags were generated using retroviral vector (pOZ-FH-C-puro, Addgene plasmid # 32516) (Kumar et al., 2009). The FLAG-HA-tagged AGO1 was immunoprecipited by HA-antibody (Abcam, # ab9110) for ChIP experiment as mentioned above.

AGO1 RIP from Chromatin Fraction

The AGO1 RIP-seq was performed following the above ChIP experiment until the last washing step as described in the protocol. The whole procedure was carried out at 4°C and all the buffers were prepared in DEPC (0.1 % (v/v) and supplemented with Superase-In (Ambion–AM2696) 10U/ml. After proteinase K treatment (0.4 μg/ml) on beads at 37°C for 30 min, the samples were processed for the reverse cross-linking at 65°C for 2 hrs. Finally, the RNAs were extracted using TRI reagent and processed for library preparation (TruSeq Stranded Total RNA Library, Illumina). The RIP-seq libraries were prepared from two replicates of chromatin-bound AGO1 associated RNAs and mock sample RNAs (control) for 100 and 400 fragment sizes. Raw sequencing reads were aligned to the UCSC human genome release hg19 using tophat2 (v2.0.14). In order to identify enriched peaks, the target and mock reads for each fragment size and for each replicate independently were first aligned. They were then used as input for piranha (v1.2.1) (Uren et al., 2012) with the following command-line options "-s -l". Only consistent peaks, identified through genomic overlap of at least 1 base were retained using BEDTools (Quinlan and Hall, 2010). Figures were generated using R and ggplot2.

RT-qPCR

Extracted RNA samples were reverse transcribed using the QuantiTect reverse transcription kit (Qiagen, Cat # 205311). cDNA from RNA and ChIP-DNA were amplified by quantitative PCR on CFX96 Real-Time PCR Machine (Bio Rad) using the SYBR Select Mastermix (Applied Biosystems, Waltham, Massachusetts, United States of America). For gene expression normalization, the geometric mean of 18S rRNA, GAPDH, and Actin-B mRNA levels, were used. For primers detail see Table S5.

Preparation of Hi-C Libraries and Generation of Contact Matrices

Hi-C experiment was carried out as previously described (Lieberman-Aiden et al., 2009; Belton et al., 2012), with minor modifications (Schoenfelder et al., 2015). Briefly, 25 million cells were fixed with 2% formaldehyde and lysed. Following HindIII digestion and biotinylation of DNA ends (Biotin-14-dATP), ligation was performed using T4-DNA ligase inside the nuclei. After de-crosslinking the DNA was purified, sheared and pull-down with streptavidin beads. Hi-C libraries were prepared for sequencing on HiSeq 4000 (Illumina). After sequencing Fastq data were processed through HiC-Pro pipeline (Servant et al., 2015) for generating contact matrices at different resolutions (1Mb, 150kb, 100kb and 20kb). We obtained a total of around 190 million valid interaction pairs, ~95 million for siCtrl and ~95 million for siAGO1 HepG2 cells (combined replicates) (Figures S7A–S7D), the two replicates in each condition showed high degree of similarity and reproducibility (Figure S7E).

Small RNA-seq

The small RNA-seq libraries were generated from total RNA with three replicates in each condition (siCtrl and siAGO1 HepG2) using Illumina TruSeq small RNA protocol. These libraries were sequenced on Illumina HiSeq2000. After QC and trimming of low quality bases and adapters, the fastq files were uploaded to the online small RNA-seq analysis tool Oasis 2.0 (https://oasis.dzne.de) (Rahman et al., 2018) for detection, differential expression, and classification of small RNAs. We identified a list of significant (p-value 0.01) differentially expressed miRNAs. For integration with CAGE-seq data, we used the mirTarBase tool (mirtarbase.mbc.nctu.edu.tw/php/) (Chou et al., 2018) to identify the targets of differentially expressed miRNAs in the list of differentially expressed genes from AGO1 knockdown CAGE-seq data.

Bioinformatics Analyses

CAGE-seq Data Analysis

The CAGE libraries were generated using RNA extracted either from chromatin or total fraction with three replicate in each condition (siCtrl and siAGO1 HepG2). These libraries were sequenced using HiSeq2000 with each single read of 50-bp length. The low quality bases and adapter were trimmed using cutadapt tool. The clean reads were then mapped on to the human reference genome hg19 from UCSC. To get the tag counts that mapped on to the genomic loci, the mapped bam files were analyzed using the R package

CAGEr (https://bioconductor.org/packages/release/bioc/html/CAGEr.html). Expression tables were generated by counting the number of mapped reads within 500 bases of an UCSC (http://hgdownload.cse.ucsc.edu/goldenPath/hg19) annotated 5 prime ends as expression from the transcript in CAGE. The number of tags for each sample was used as input counts and uploaded to the DESeq2 a Bioconductor package (https://bioconductor.org/packages/release/bioc/html/DESeq2.html) for differential gene expression calculation. The up and down regulated genes were tabulated with a significance FDR threshold of 0.05.

For enhancer RNAs (eRNAs) identification, CAGE expression (chromatin and total) data was used as described previously (Andersson et al., 2014). The CAGE identified enhancer loci were then used for downstream analysis. The common CAGE predicted eRNAs between siCtrl and siAGO1 cells were selected. These common eRNAs (tpm) were then used for comparison of expression dynamics between siCtrl and siAGO1 cells using heatmapper (Babicki et al., 2016).

To identify CAGE-defined eRNAs that overlap with AGO1-bound enhancer regions, eRNA loci were intersected with AGO1 ChIP-seq peaks using bedtools intersection (Quinlan and Hall, 2010). Similarly, intersection with ENCODE ChIP data sets (H3K4me1 and H3K27ac) and HepG2 GRO-seq (Bouvy-Liivrand et al., 2017) was performed. Some randomly selected eRNAs that overlapped with all data sets (ChIP-seq: AGO1, H3K4me1, H3K27ac and GRO-seq peaks) were further validated qPCR analysis in control and actinomycin D treated cells.

ChIP-seq Data Analysis

After sequencing ChIP-seq reads of quality score less than 20 and length of 30bp were removed using sickle (http://www.citeulike.org/user/mvermaat/article/13260426). We aligned the reads to the human genome assembly GRCh37 (hg19) using Bowtie (Langmead and Salzberg, 2012) (version 2.2.5) with default parameters, and results were converted to sorted bam using samtools (Li et al., 2009) (version 1.2). HMCan peak calling tool (Ashoor et al., 2013) was used for ChIP-seq peak calling. This tool is used for cancer cells to normalize reads for GC and copy number variation. Peak calling was then followed by irreproducibility discovery rate (idr) analysis (Li et al., 2011). For peaks annotation, we used GENCODE (Harrow et al., 2012) (version19) annotation of the genome. ChIP-seq peaks were annotated using Bedtools (Quinlan and Hall, 2010) and BEDOPS (Neph et al., 2012). Gene expression was measured as the sum of normalized CAGE tags within 500 pb from TSS. For integration with ChIP-seq, CAGE signals around ChIP-seq peaks were computed using bwtools (Pohl and Beato, 2014) (version 2.17).

Hi-C Data Analysis

Differential Interaction Analysis

Genome-wide Hi-C matrices were loaded to the R package diffHiC (Lun and Smyth, 2015) (version 1.6.0) to identify differential interactions between siAGO1 and siCtrl cells at different resolutions. Those interacting pairs of bins with an average read count less than 5 (considering all replicates) were filtered out. The LOESS method was used to normalise counts between libraries. The interacting pair of bins with a FDR value smaller than 0.05 were considered significant.

Identification of Topologically Associated Domains (TADs)

Columns with low number of counts in the genome-wide Hi-C matrices at 100 kbp resolution were filtered out using TADbit (version 0.2.0.23) (Serra et al., 2017) setting the parameter "min_count" to 10. Since TADbit fits the column count distribution into a polynomial distribution, columns with a number of counts smaller than the first antimode of the distribution, which cannot be smaller than the "min_count" parameter, are filtered out. Then, 100 kbp genome-wide matrices were normalized by visibility (1 iteration of ICE). Afterwards, the breakpoint detection algorithm of TADbit that returns the optimal segmentation of the chromosome under BIC-penalized likelihood was applied in order to identify Topologically Associating Domains (TADs). Hi-C matrices at 40 kbp resolution were processed per chromosome instead of genome-wide.

Identification of Compartments

For compartment profiling, first columns with low number of counts in the genome-wide Hi-C matrices at 100-kbp resolutions were filtered out using TADbit (version 0.2.0.23) setting the parameter "min_count" to 10. Then, 100 kbp genome-wide matrices were normalized by the expected interactions at a given distance and by visibility (1 iteration of ICE). The correlation analysis was performed with TADbit tool to obtain the first eigenvector. In-house scripts computed A/B compartments from the first eigenvector, using 0 as threshold to differentiate both compartments and genes with a basemean expression higher than 20 as active marks to label compartments. Hi-C matrices at 40-kbp resolutions were processed per chromosome instead of genome-wide.

Heatmaps and Multi-Track Plots

The raw and normalized corrected matrices were plotted using hicPlotMatrix of HiCExplorer (version 1.3) (http://hicexplorer.readthedocs.io/en/latest/index.html). Corrected matrices underwent a low-count bin filtering and ICE normalization (500 iterations) prior to plotting. Multi-track plots were generated using HiCExplorer hicPlotTADs.

TAD Compartment Switching

TADs identified in siCtrl cells were intersected using the bedtools intersect with the first eigenvector of siCtrl and siAGO1 cells. Positive eigenvector values were attributed to A compartments, while negative eigenvector values were attributed to B compartments. For each TAD and condition, the mean of the values of the corresponding eigenvector was calculated. TADs having a change in the sign of the calculated means were designated as TADs that switched compartments.

QUANTIFICATION AND STATISTICAL ANALYSIS

All NGS data were analyzed using specific pipelines with statistical setting described in the STAR Methods. The significance of statistical analyses was computed either with Permutation tests, Mann–Whitney–Wilcoxon test, or t test. The quantification and statistical details (p value and FDR thresholds, and the value of n) of each analysis can be found in the respective figure legends, Method Details, and within the main manuscript.

DATA AND CODE AVAILABILITY

The high throughput sequencing data including CAGE-seq, ChIP-seq, small RNA-seq and Hi-C-seq have been deposited at the Sequence Read Archive (SRA, http://www.ncbi.nlm.nih.gov/sra/), which is hosted at the NCBI, under the accession number SRA: PRJNA398595. The AGO1 RIP-seq (chromatin-bound) data has been deposited at SRA under the accession number SRA: PRJNA543746.